

CORROSION OF ALUMINUM METAL IN CONCRETE – A CASE STUDY

Dipayan Jana¹ and David G. Tepke²

¹**Construction Materials Consultants, Inc. 4727 Rt. 30, Greensburg, PA 15601 USA, and**

²**Sutton-Kennerly & Associates, Inc. 300 Pomona Drive, Greensboro, NC 27407 USA.**

Abstract

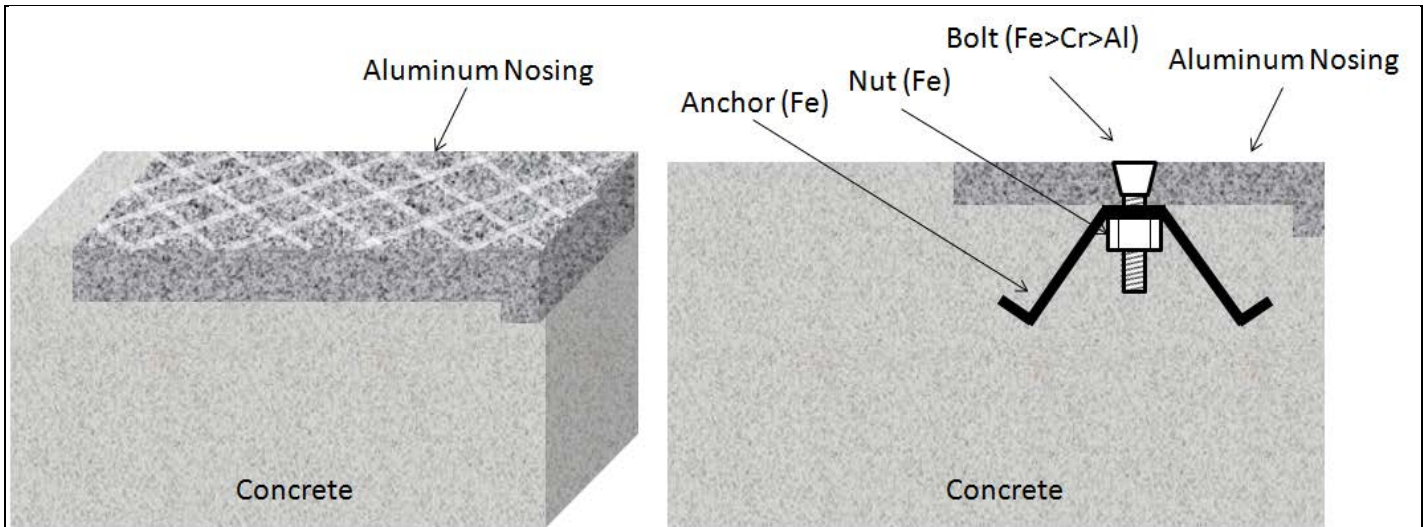
Galvanic corrosion of steel-anchored aluminum nosing in outdoor portland cement concrete stairs caused debonding and cracking of the nosing, and, cracking and spalling of the adjacent concrete. Chloride-induced corrosion of embedded steel anchors in concrete has created iron oxide corrosion products and associated cracking in concrete. Chloride-induced galvanic corrosion of aluminum nosing at the locations of steel anchors has created more severe distress due to corrosion (reduction in thickness) of the nosing. Aluminum corrosion in the presence of moisture, hydroxyl and chloride ions from concrete formed a gelatinous mass of hydrated aluminum corrosion products, and associated aluminum hydroxide crystals (boehmite, bayerite, and gibbsite). A characteristic banded microstructure of sheet-like friable corrosion products of aluminum metal is detected, due to layer-by-layer advancement of corrosion, which consists of alternating layers of soft hydrated aluminum deposits and hard silicon-rich phases (the latter from silicon carbide grains embedded in nosing during manufacturing). The bottom 1 mm zone of nosing shows a corrosion microstructure where silicon-rich blades were distributed in a hydrated aluminum mass, which eventually grades into the sheet-like severely corroded metal, as described. Formation of a gelatinous mass of hydrated aluminum products and associated expansion is responsible for the nosing debonding and associated cracking of concrete, which is similar to concrete cracking by formation of alkali-silica reaction gel. Possibility of galvanic corrosion of aluminum in concrete and corrosion-related distress, especially in contact with steel and chloride, therefore, should be minimized by using a protective insulating coating on the surface of aluminum nosing in contact with concrete and embedded steel.

Introduction

Corrosion of aluminum metal in a portland cement concrete is well-known for more than fifty years causing deterioration or collapse of aluminum conduit, and cracking and spalling of concrete [1-6]. Studies done in the 1950's and 1960's [1, 2, 6] established that severe corrosion of aluminum commonly occurs when it is embedded in concrete that contains calcium chloride and steel that is electrically connected to the aluminum (*galvanic corrosion of aluminum coupled to steel*). Corrosion of aluminum can still occur in the alkaline (high pH) environment of portland cement concrete, from alkali hydroxide and moisture in the pore solution (*alkali hydroxide attack of aluminum*), without the presence of chloride, or coupling to steel, although such corrosion may not be as severe as in the cases of galvanic corrosion of aluminum from coupling with steel in the presence of chloride [2, 5]. The presence of chloride has also been reported to cause aluminum corrosion in the alkaline environment of portland cement concrete, even in the absence of steel (*chloride attack of aluminum*), which, again, is not generally reported as being as severe as the case of chloride-induced galvanic corrosion of aluminum coupled to steel (some other studies reported no apparent corrosion of aluminum in concrete containing calcium chloride and no coupling to steel, [7]. McGeary [6] concluded that stray currents can sustain corrosion and associated damage, especially in the presence of chlorides. The literature suggests that the presence of moisture, level of alkalinity, presence of chlorides, galvanic coupling between steel and aluminum and associated ratios of connected metal areas, and stray currents are all factors that may affect aluminum corrosion, with the associated corrosion rates and damage being dependent on the interactions of these factors. Aluminum corrosion evolves hydrogen gas, produces various hydrated aluminum corrosion products with subsequent reduction in strength of the metal, and causes expansion, cracking, and spalling of adjacent concrete from the formation of expansive aluminum corrosion products. This may reduce the structural capacity and permit additional moisture into the concrete to facilitate further corrosion. To protect against corrosion, some have recommended the use of protective inert or insulating coatings when concrete may be exposed to chloride (e.g., chloride-containing deicing agents or calcium chloride admixture) [2, 3, 6, 8]. ACI 318-08 [9] Building Code Requirements for Structural Concrete prohibits the use of uncoated or uncovered aluminum in structural concrete and the use of water or admixtures with deleterious amounts of chloride ions when aluminum is embedded in concrete.

Background

The present study involves corrosion of aluminum nosing anchored on concrete stairs in a parking facility in North Carolina, where the stairs, though partially covered, are open to the outdoor environment of moisture, cyclic freezing and thawing, and deicing salts on one or more sides in North Carolina. Aluminum nosings were reportedly: (a) manufactured with silicon carbide granules embedded into the walking surface while the metal matrix was in a molten state; and (b) approximately 96 in. long, 2³/₄ in. wide, and 1/4 in. thick with anti-slip treads anchored to the concrete stair noses with embedded steel wing anchor and steel nuts and bolts at approximately 12 in. anchor intervals, in the plastic state of concrete. Figure 1 shows the configuration of aluminum nosing anchoring, along with elemental analyses of four different metals (aluminum nosing, steel anchor, nut and bolt) in a sample done by x-ray elemental analyses in a scanning electron microscope.



Atomic Weight Percent of Elements in Four Metals Determined from SEM-EDS Analyses

Elements	Aluminum Nosing					Steel Wing Anchor	Bolt	Nut
	Top Exposed	Middle 1	Middle 2	Bottom Sound	Average			
Fe	0.1	0.3	0.2	0.3	0.2	85.2	49.8	86.6
Al	76.4	74.9	75.8	77.6	76.2	9.8	13.5	8.9
Si	18.5	18.3	18.5	16.2	17.9	4.2	3.6	3.9
Cr	0.0	0.0	0.0	0.0	0.0	0.5	22.3	0.3
Ni	0.0	0.0	0.0	0.0	0.0	0.0	8.3	0.0
Cu	1.5	1.9	2.3	1.9	1.9	0.0	2.2	0.0
O	2.8	3.6	2.3	3.4	3.0	0.2	0.2	0.2

Note: Elements greater than 10% are shaded and shown in the above diagrams for different metals

Steel Anchored Aluminum Nosing = Iron – Aluminum Metal Coupling

Figure 1: Schematic diagram of aluminum nosing and its attachment to concrete stair by steel wing anchor, bolt, and nut. The table shows SEM-EDS analyses of compositions of metals.

As can be seen from the elemental analyses: (a) the aluminum nosing contains a major amount (i.e. >75%) of aluminum, and subordinate amount (15 to 20%) of silicon from the embedded silicon carbide granules; (b) the steel wing anchor contains a major amount (i.e. >85%) of iron and subordinate amounts (i.e. 4-10%) of aluminum and silicon; (c) the bolt used to attach the nosing to the anchor contains a major amount (i.e. 45 to 50%) of iron and subordinate amounts (i.e. 10 to 25%) of aluminum and chrome; and, (d) the nut completely embedded in concrete contains a major amount (i.e. >85%) of iron and minor amounts (i.e. 3 to 9%) of aluminum and silicon.

The anchoring process itself, therefore, created an excellent aluminum-iron alloy-steel coupling in an outdoor environment of moisture and salts in the concrete stairs, which has set the stage to initiate a galvanic action of dissimilar metals in the presence of chloride-based deicers reportedly applied to the stairs.

Field Evidence of Distress

A detailed field investigation was done to examine the nosing failures at several locations of the stairs. The investigation included evaluation of three stair towers. In many stairs, aluminum nosing show debonding or separation from the concrete surface (bowing), and fracturing (the latter especially at the locations of steel anchors, Figure 2). Separations were hairline up to $\frac{3}{16}$ in. or more in width. Extent of distress varied from minor to extensive with cracked nosings and significant spalls.

Undersides of debonded nosing plates show (preferentially located at the places of steel anchors):

- (a) Severe corrosion of metal in terms of loss of the cross sectional thickness (e.g., from 7.9 mm maximum to 6.1 mm at the location of steel anchor in one nosing sample), and
- (b) Ring-textured corrosion products (see Figure 2) concentric around the corroded steel nuts, consisting of reddish brown iron oxide corrosion products of steel nut/bolt/anchor at the center, dark greenish gray mass of highly corroded, fragile, sheet-like metal consisting of alternating bands of white corrosion products and gray metal hydrates, and an outer ring of soft, powdery, white corrosion products from the nosing.

No protective coating between the aluminum and concrete or aluminum and iron-based anchoring components was observed.

Concrete at the locations of steel anchors show cracking and spalling. Cracks sometimes are filled with white corrosion products from the nosing and/or reddish brown corrosion products from the steel anchor/nut/bolt. Portions of the nosing underside in between the steel anchors are present mostly in sound condition with no noticeable corrosion compared to the areas adjacent to the anchor locations.



Figure 2: Field photographs of corrosion and debonding of aluminum nosing and associated concrete distress.

Samples

Based on the field survey, samples were taken from two representative locations of the stairs, where the aluminum nosing shows severe corrosion, fracturing, formation of white corrosion products at the undersides, and cracking of concrete – all preferentially located at the areas of steel anchors.

Figure 3 shows the two samples received for detailed laboratory studies. The first sample, SKA 3-1, was taken by dry saw-cutting a 24 in. long \times 5 $\frac{1}{4}$ in. wide \times 5 in. thick section of a stair containing a 30 in. long \times 3 in. wide \times $\frac{1}{4}$ in. thick aluminum nosing (shown in the top left field photo), where the aluminum nosing shows separation (bowling) from concrete, and severe corrosion at its underside, at the two locations of steel anchor. As shown in the bottom left column photo, the underside of the nosing shows severe and preferential corrosion of metal at the locations of steel anchor, white corrosion products forming around the hole in the metal for steel bolt, and cracking of concrete at the corroded locations.

The second sample, SKA 3-2, consists of a portion of a corroded, debonded aluminum nosing (shown in the top right composite field photo), and several plastic bags of loose powdery to fragmented pieces of corrosion products of nosing collected from around the steel anchors. Of particular importance in this sample are: (a) the white corrosion products from metal nosing, (b) loose pieces of sheet-like masses of severely corroded metal consisting of alternating bands of white corrosion products and dark corroded metal, and (c) the underside of the corroded aluminum piece.

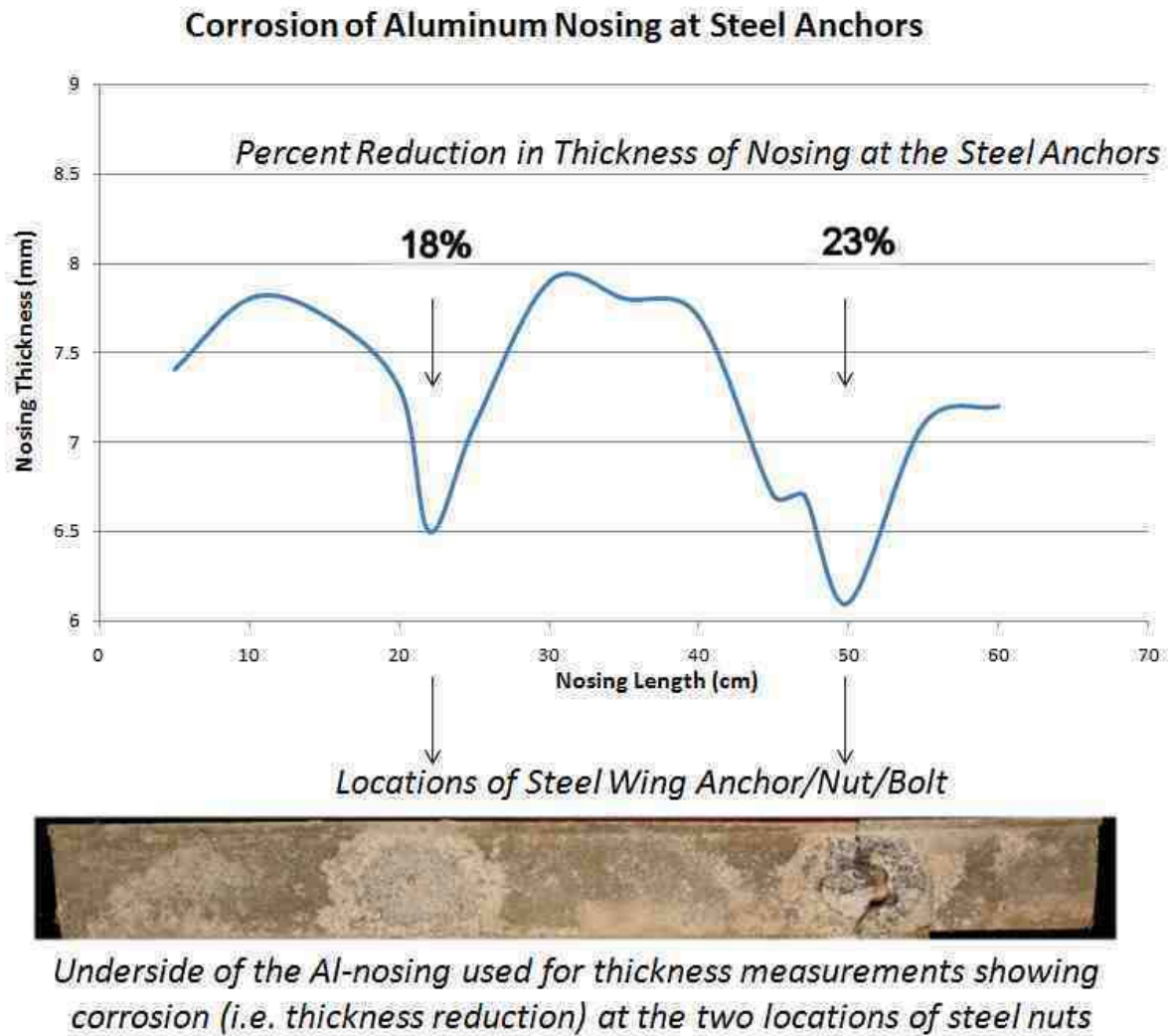


Figure 3: Two samples, SKA 3-1 and 3-2 from two different locations of stairs that show aluminum nosing corrosion and associated concrete cracking and spalling.

The right composite photos in Figure 3 show field locations of debonding and associated corrosion products of nosing for Sample SKA 3-2. The middle photo in the bottom row of this right composite set shows a typical ring-structure of corrosion consisting of dark gray colored somewhat hard corrosion products formed around a steel nut, which is surrounded by a layer of soft, powdery white corrosion products. The underside of nosing at this location shows severe corrosion and remains of the white deposits. Notice the nosing was fractured at this location due to significant thickness reduction of metal by corrosion. Small pieces of these corrosion products in the field were carefully collected in plastic bags for detailed laboratory examinations.

Reduction in Metal Thickness by Corrosion of Aluminum Nosing at the Locations of Steel Anchors

A measurement of nominal maximum thickness of the debonded aluminum nosing in SKA 3-1 by a digital micrometer shows severe preferential corrosion of nosing at the locations of steel anchors, which is measured to be ~18 to ~23 percent loss of thickness by corrosion of the metal, as shown in the graph in Figure 4. Such a thickness reduction by corrosion has caused loss of strength of the metal, and cracking and debonding of the nosing at many stairs.



SKA 3-1

Figure 4: Reduction in cross sectional thickness of aluminum nosing at the locations of steel anchors.

Methodology

The samples were examined by using the methods and procedures of ASTM C 856 "Standard Practice for Petrographic Examination of Hardened Concrete," which includes: (a) preparation of pulverized, fractured, saw-cut, lapped, and thin sections of nosing, concrete, and corrosion products for optical and scanning electron microscopy, and x-ray diffraction studies, (b) optical microscopy of as received, fractured, sectioned, lapped, polished, and thin sections of nosing, concrete, and corrosion products in low power stereomicroscope and high power petrographic microscope, (c) scanning electron microscopy (backscatter and secondary electron imaging) with energy-dispersive x-ray elemental microanalyses (SEM-EDS) of metals and corrosion products, and (d) x-ray diffraction studies of corrosion products.

Additionally, acid-soluble chloride analyses were done from the top and bottom ends of concrete stair in one sample, which detected 0.655 and 0.006 percent chloride by mass of concrete at the top and bottom ends of concrete, respectively, where more than one-hundred times higher chloride content at the top of the stair (directly adjacent to the nosing) compared to that at bottom is indicative of exposure to chloride-containing deicing salts at the surface of concrete, which has created an ideal environment for galvanic corrosion of aluminum nosing in contact with steel anchor and nut.

Sample SKA 3-1: A Section Through Steel Bolt, Anchor, Nut, and Aluminum Nosing

Figure 5 shows a clear epoxy-impregnated lapped cross section (top photo, carefully sectioned through a steel bolt and nut), and a blue dye-mixed epoxy-impregnated polished cross section (bottom photo) of small portions saw-cut from around a corroded nosing/anchor area in the sample. Important features in these figures include:

- (a) Complete separation of nosing from concrete,
- (b) Reddish brown iron oxide corrosion products and associated concrete cracking around the corroded steel component,
- (c) Layered-type or banded corrosion products of aluminum nosing (described in detail, later determined to be amorphous hydrated aluminum) situated around the steel anchor as well as at the interface between the nosing and concrete, and
- (d) Aluminum-iron alloy-steel coupling of nosing and anchor/bolt/nut where compositions of metals are given before.

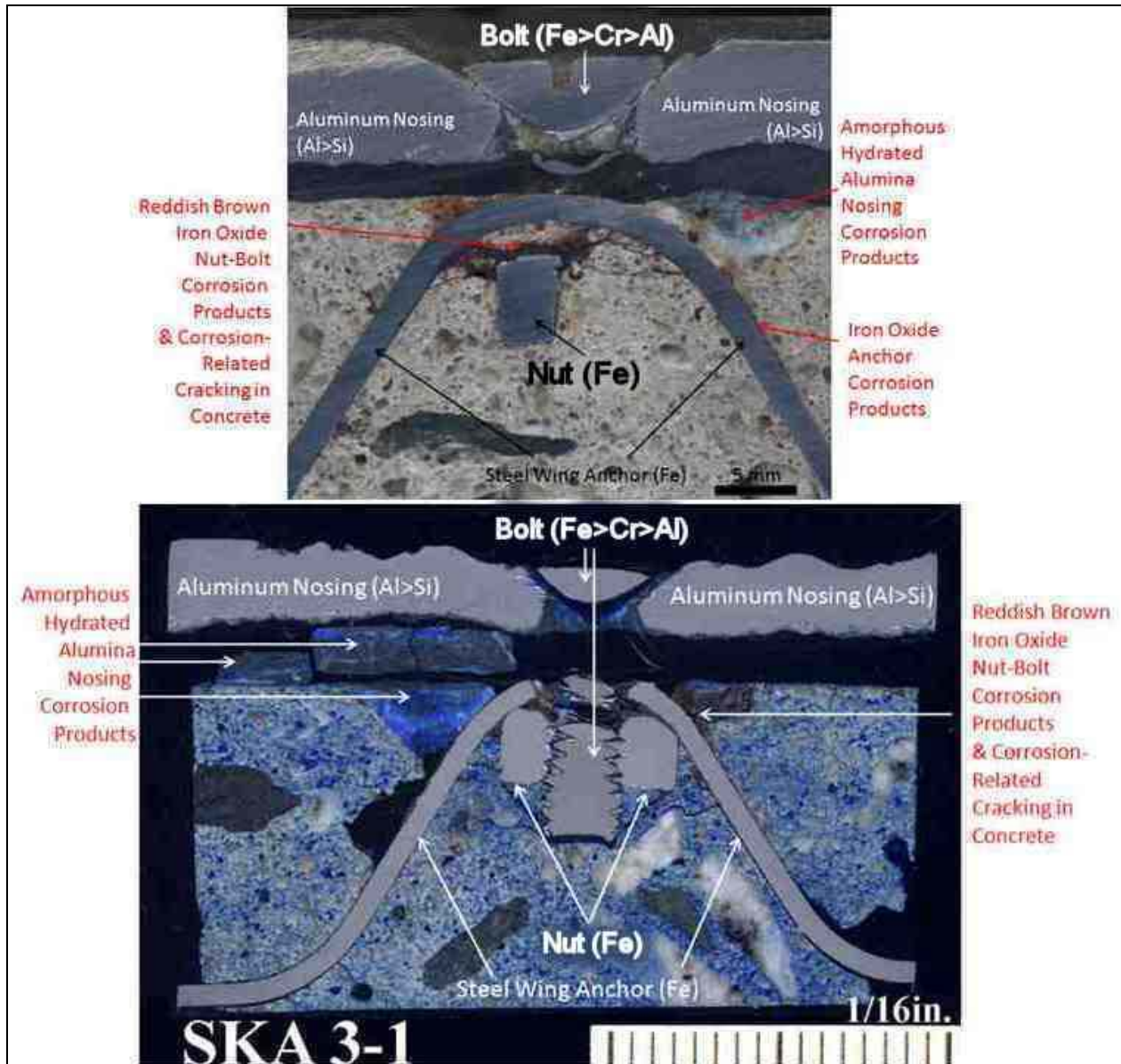


Figure 5: Lapped (top) and blue dye-mixed epoxy impregnated polished cross section (bottom) of SKA 3-1 through aluminum nosing, steel anchor, nut, and bolt showing corrosion of nosing and anchor materials.

Corrosion Microstructure of Aluminum Nosing at the Nosing-Concrete Interface in SKA 3-1

Figure 6 shows backscatter electron (BSE) images of cross section of aluminum nosing in Sample SKA 3-1, where the top left photo shows the bottom half of the metal including the “corrosion zone” at the very base (e.g., boxed) that was in contact with portland cement concrete stairs.

The overall microstructure of metal body above the bottom corrosion zone is more or less homogeneous with small-scale heterogeneities of very fine areas or spots of silicon-rich areas (from the silicon carbide grains embedded in the molten aluminum matrix) uniformly

distributed in the overall aluminum matrix. Apart from this small-scale compositional variations between the silicon-rich spots and aluminum matrix, approximately 100 to 200 micron size raster-mode compositional analyses of the metal by SEM-EDS, at the top exposed location, in mid-depth location, and at the bottom sound location away from the corrosion zone show more or less similar compositions (in atomic weight percent) of ~75% Al, 18% Si and <2.5% Cu (see Figure 1 for metal compositional analyses).

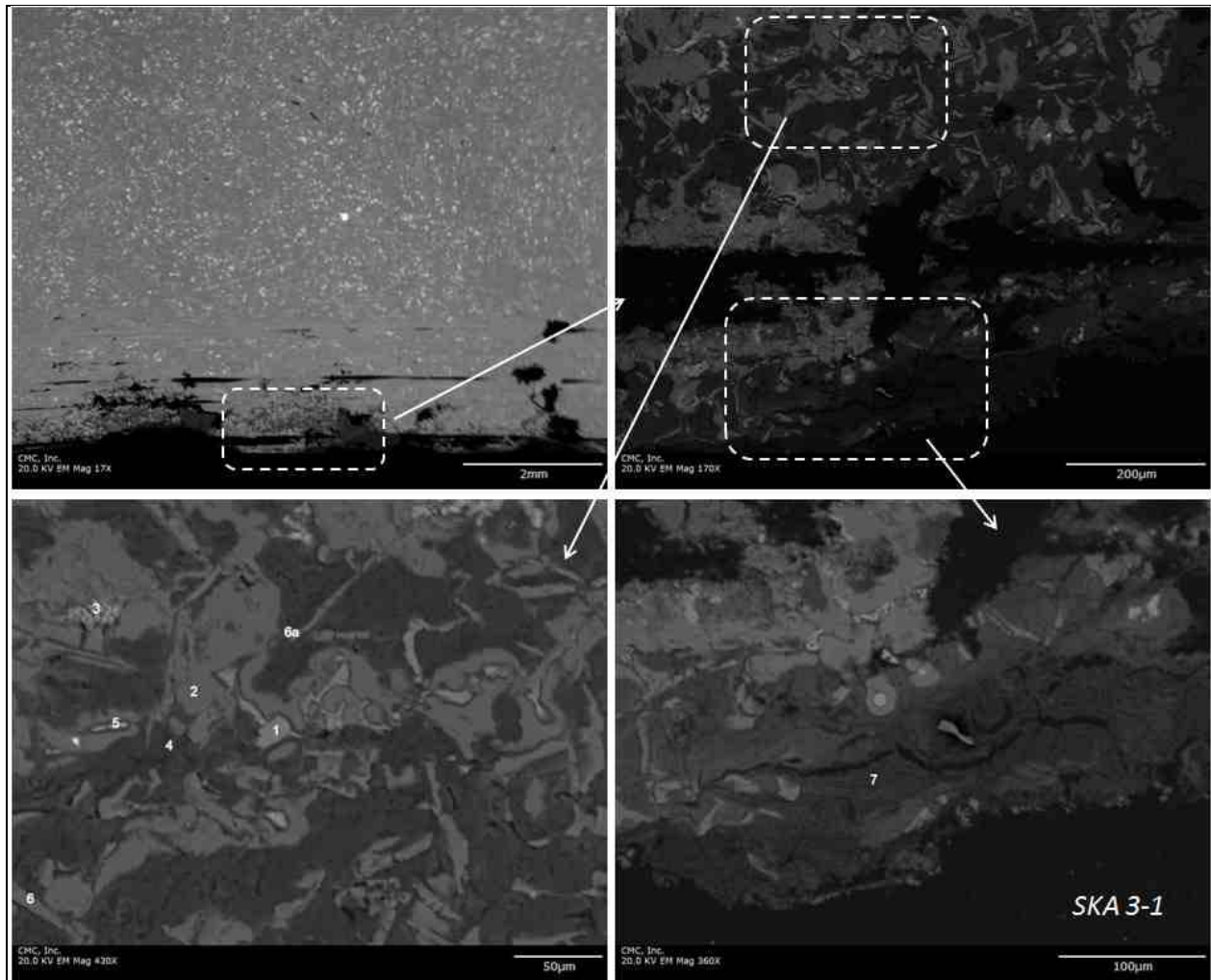


Figure 6: Backscatter electron images of cross section of an aluminum nosing, showing corrosion microstructure along its base near the nosing-concrete interface.

The very bottom 1 mm thick zone of the aluminum nosing is the “corrosion zone” (the top right photo in Figure 6, which is an enlarged view of the boxed area in the top left photo), where the overall somewhat “monotonous” microstructure of silicon-rich spots in aluminum matrix changes into a complex microstructure consisting of at least 6 to 7 different phases with compositions different from the overall metal in the body, above the corrosion zone. The bottom two photos in the figure are enlarged views of two areas of this corrosion zone, where

six to seven different spots with phases of different compositions are detected. The following Figure 7 is an enlarged view of the bottom left photo, where six different phases are detected. The major phase (the darkest phase in BSE image) is aluminum hydroxide (Al and O as major peaks in SEM-EDS spectra, e.g., Spot Nos. 4 and 7) with various incorporations of Ca, Mg, Cl, S, Cu, Si, etc. The brightest areas (e.g., Spot# 1) are of Al-Si-Fe composition (e.g., >70% Al, 10-15% Si, 10% Fe), where incorporation of iron (possibly from the steel nut/bolt/anchor) has caused increased brightness in BSE-image. The blade-shaped phases (e.g., Spot Nos. 6 and 6a) are rich in silicon, from the original silicon carbide grains, with 85 to 90% Si and 5 to 10% Al. The bright dendritic-textured and stout rod-shaped phases incorporated copper (e.g., > 60% Al, > 25% Cu). The overall gray areas in the matrix (e.g., Spot# 2) are very rich in aluminum (e.g., >90% Al, 2.5% Si, 1% Cu). Therefore, the “corrosion zone” shows: (a) an overall shapeless hydrated aluminum matrix (the darkest areas) with (b) major amounts of irregularly-shaped aluminum-rich areas (gray areas), (c) minor amounts of blade-shaped silicon-rich phases from embedded silicon carbide grains and bright Al-Si-Fe areas, and (d) trace amounts of dendritic or stout rod-shaped Al-Cu alloy phases.

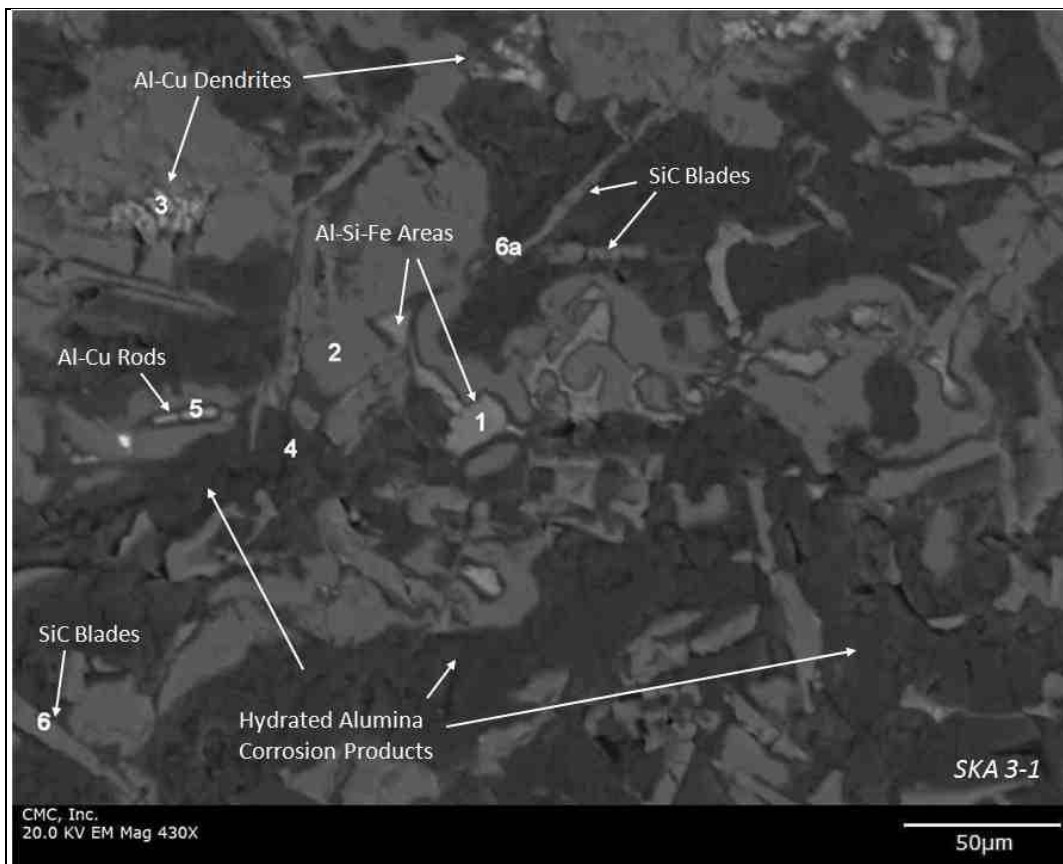


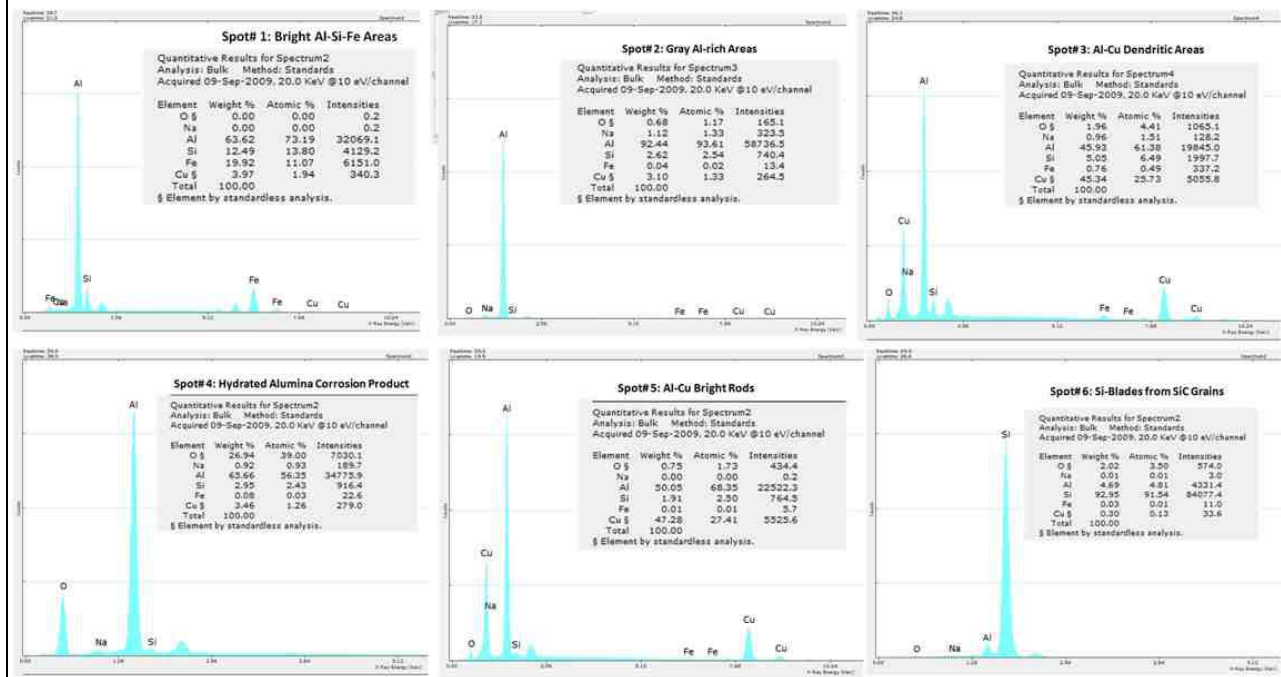
Figure 7: Different phases from corrosion of aluminum nosing.

The following Table and SEM-EDS spectra show detailed compositional analyses of all these phases in the bottom 1-mm thick corrosion zone of the aluminum nosing.

Chemical Compositions (in Atomic Weight Percent) of Different Areas Near the Base of Aluminum Nosing in the Corroded Region

Elements	Spot# 1 (Bright Area)	Spot# 2 (Gray Area)	Spot# 3 (Dendritic Area)	Spot# 4 (Dark Area)	Spot# 5 (Bright Rods)	Spot# 6 (Si-Blades)	Spot# 6a (Si-Blades)	Spot# 7 (Dark Area)
Al	73.2	93.6	61.4	56.3	68.3	11.3	4.8	63.6
Si	13.8	2.5	6.5	2.4	2.5	86.8	91.5	3.8
Fe	11.1	0.0	0.5	0.0	0.0	0.0	0.1	0.0
Cu	1.9	1.3	25.7	1.3	27.4	0.3	0.1	0.3
O	0.0	1.1	4.4	39.0	1.7	1.4	3.5	32.2
Comments on Possible Phases	<i>Al-Si-Fe Metal Area (Fe-infiltration in Al-Si Nosing)</i>	<i>Al-rich Area of Metal</i>	<i>Al-Cu Alloy in the Metal</i>	<i>Hydrated Alumina Corrosion Product of Metal</i>	<i>Al-Cu Alloy in the Metal</i>	<i>Si-Rich Blades in Metal from SiC Grains</i>	<i>Si-Rich Blades in Metal from SiC Grains</i>	<i>Hydrated Alumina Corrosion Product of Metal</i>

SEM-EDS Spectra & Chemical Compositions (in Atomic Weight Percent) of Different Areas Near the Base of Aluminum Nosing in the Corroded Region



Two Types of Corrosion Products in SKA 3-1

Petrographic examinations of blue dye-mixed epoxy-impregnated thin section of SKA 3-1 (from the top right polished block in Figure 8) detected two different types of corrosion products (from two different metals) in the concrete and at concrete-nosing interface.

The first one is reddish brown iron-oxide based corrosion products (the top, middle, and bottom right column photos in Figure 8) from corrosion of steel anchor and nut embedded in concrete, in the presence of chloride, oxygen, and moisture in concrete – the common chloride-induced corrosion of steel in concrete, which has caused some local macro and micro-cracking in concrete adjacent to the anchor and nut, and migration of corrosion products along the cracks. Apart from some local cracking in concrete from expansions associated with formation of steel anchor/nut corrosion products in concrete, such a steel corrosion process itself is judged not to have caused the reported separation of nosing plates from the concrete stairs.

The second one is white deposits of aluminum nosing corrosion products, which occur as soft, powdery to flake-like deposits, often present as outer rings around reddish brown corrosion products of steel nuts, (e.g., see Figure 2), at and around the locations of corroded steel, where corrosion (thickness reduction) of aluminum nosing is maximum. The bottom surface of nosing at the location of steel anchor shows severe corrosion, and, formation of flaky or sheet-like masses of soft, friable corroded metal hydrates with alternating bands of white deposits and dark hydrated aluminum layers (Figures 8 and 9).

The white deposits (appear blue in Figure 8 due impregnation with a blue dye-mixed epoxy) are optically isotropic, indicating the gelatinous or amorphous to crypto or microcrystalline nature (see the left column photos in Figure 8). The microstructure of these white deposits of aluminum corrosion products are fascinating, showing a distinct banded texture of alternating layers of small, stout, prismatic dark gray, brown-to-black crystals aligned in a dense, dark, hard layer (which are determined to be silicon-rich phases from the embedded hard silicon carbide grains in the soft aluminum matrix) and alternating colorless or light-colored isotropic layers of gelatinous hydrated aluminum mass.

The white deposits are present both on the surface of concrete directly adjacent to the corroded steel anchor/nut and aluminum nosing interface, and also at the interface between the nosing and concrete surface, as soft layered deposits, significantly softer than the metal itself.

The gelatinous nature of the white deposits and their presence at the nosing concrete debonded interface indicate their potential expansion in the presence of moisture, which is judged to have caused the nosing debonding.

Similar white corrosion products were described in corrosion and collapse of aluminum conduit embedded in concrete in the studies by Monroe and Ost [Ref. 2], who determined their

compositions from X-ray spectrographic analyses to be approximately 40 percent aluminum, 20 percent chlorine, and less amounts of other elements. The present study detected around 20 to 30 atomic percent aluminum, 60 to 65 atomic percent oxygen, and minor amounts of silicon, calcium, magnesium, chlorine, etc.

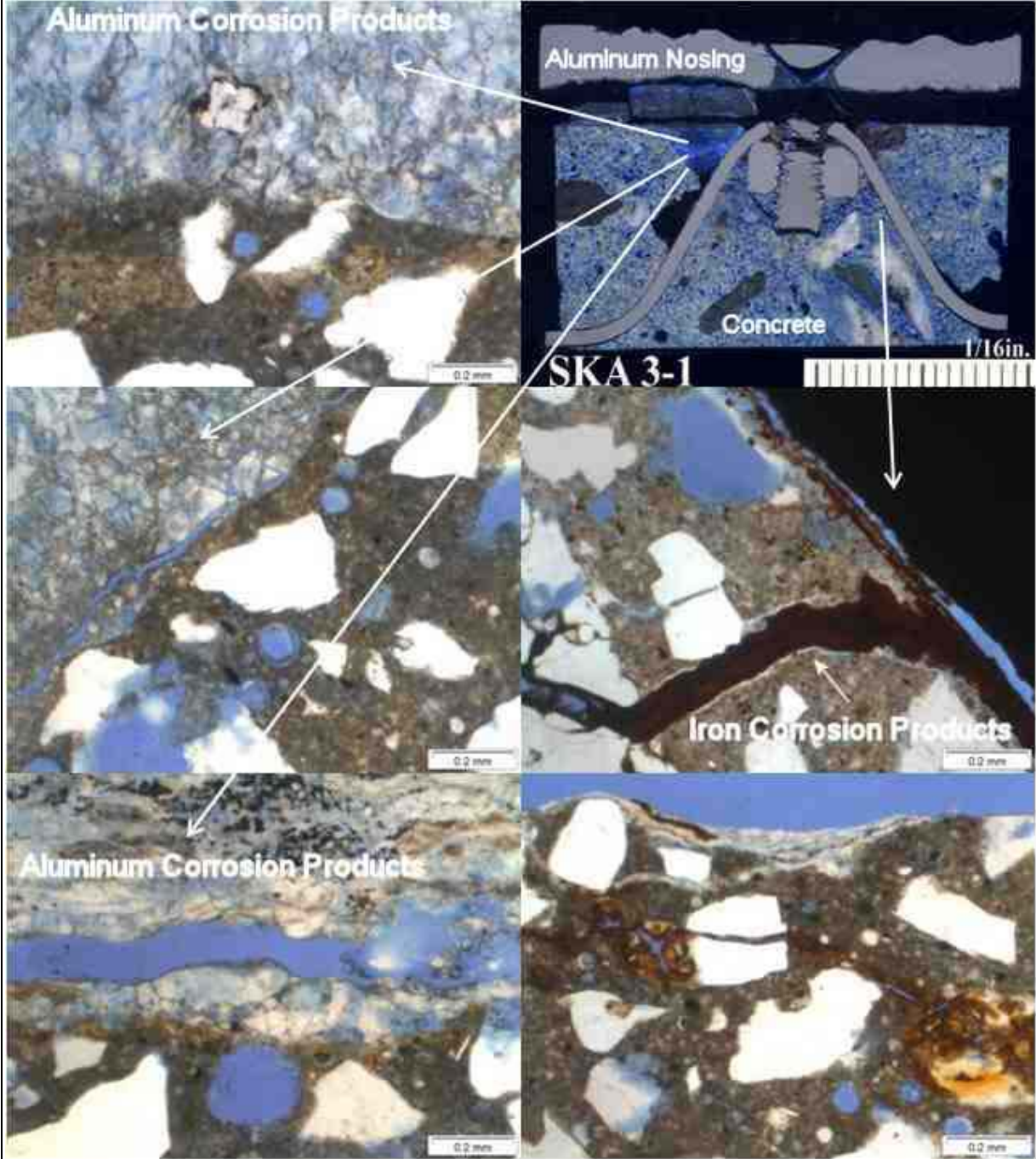


Figure 8: Photomicrographs of thin section of SKA 3-1, sectioned through iron-based anchor, nut, bolt, and aluminum nosing showing two types of corrosion products – a reddish brown product associated with corroded steel anchor, and a white (appears blue in the photo from blue epoxy) banded-type product from corroded aluminum nosing.

Banded & Gelatinous Microstructure of Aluminum Corrosion Products in SKA 3-1

Figure 9 shows transmitted-light photomicrographs of blue dye-mixed epoxy-impregnated thin section of SKA 3-1 (of the block shown in the bottom photo of Figure 5 and top right photo in Figure 8). The photos were taken from the aluminum nosing corrosion products situated in the debonded interface between the nosing and concrete surface. Due to the soft, friable nature of the white deposits that formed from nosing corrosion, an epoxy-impregnation step was essential to improve the integrity prior to thin sectioning. The photos were taken by using a stereomicroscope where white light was transmitted from the base through the thin section.

The characteristic texture of nosing corrosion products, as mentioned before, is its banded nature with alternating dark and light-colored bands (ranging in thickness from 0.05 to 0.5 mm), where the dark bands are enriched in fine, stout prismatic or irregularly-shaped, isotropic masses of silicon-rich phases (less than 10 to 50 microns in length) from the embedded silicon carbide grains in the metal, and the light bands are enriched in hydrated aluminum corrosion products. The microstructure is indicative of preferential corrosion of the overall aluminum matrix leaving silicon-rich residues as bands alternating with hydrated alumina products.

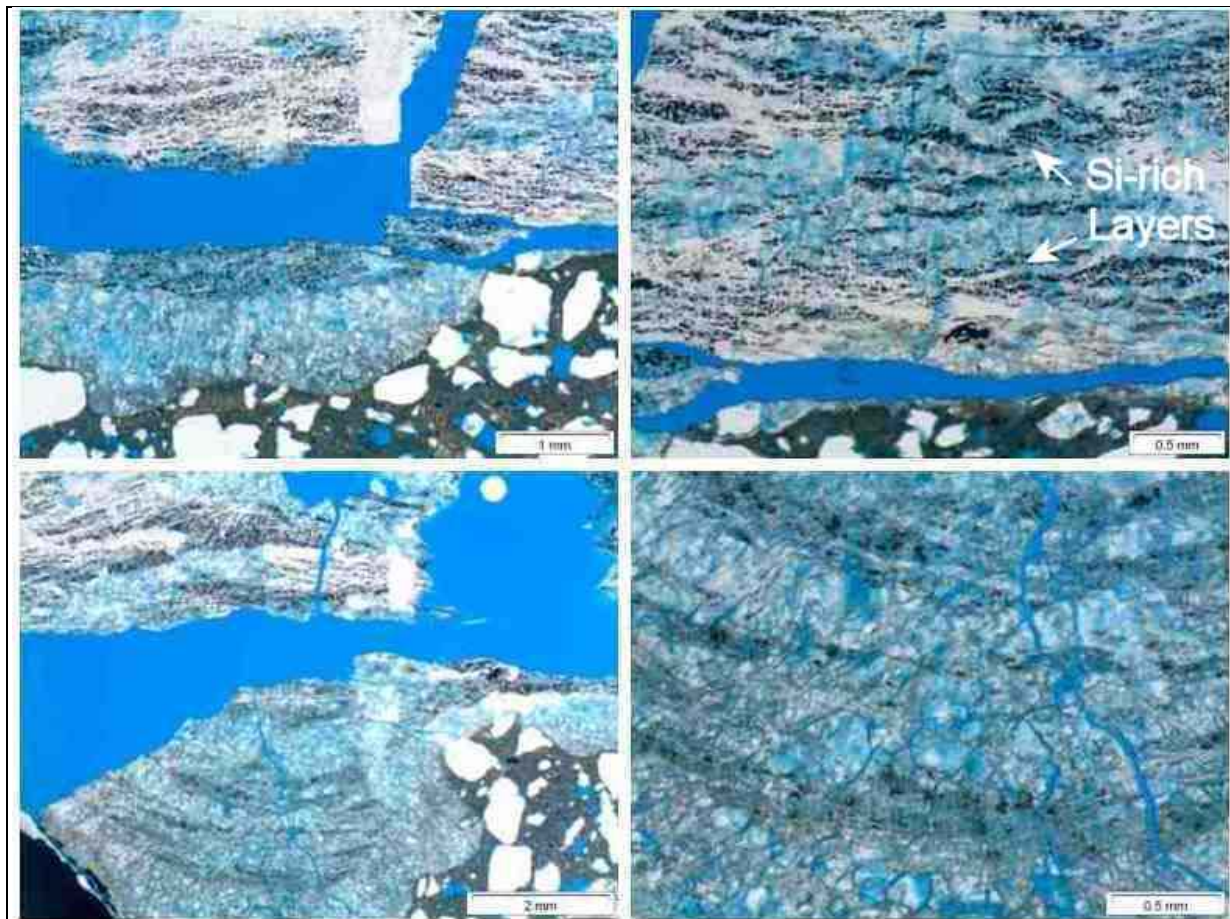


Figure 9: Photomicrographs of thin section of corroded nosing pieces showing characteristic banded nature of corrosion products consisting of alternating dark and light bands.

Figure 10 shows backscatter electron image and corresponding x-ray elemental maps for silicon and aluminum, where alternate bands of silicon-rich areas (consisting of fine, prismatic or irregular shaped silicon-rich phases) and silicon-poor aluminum rich areas are distinct.

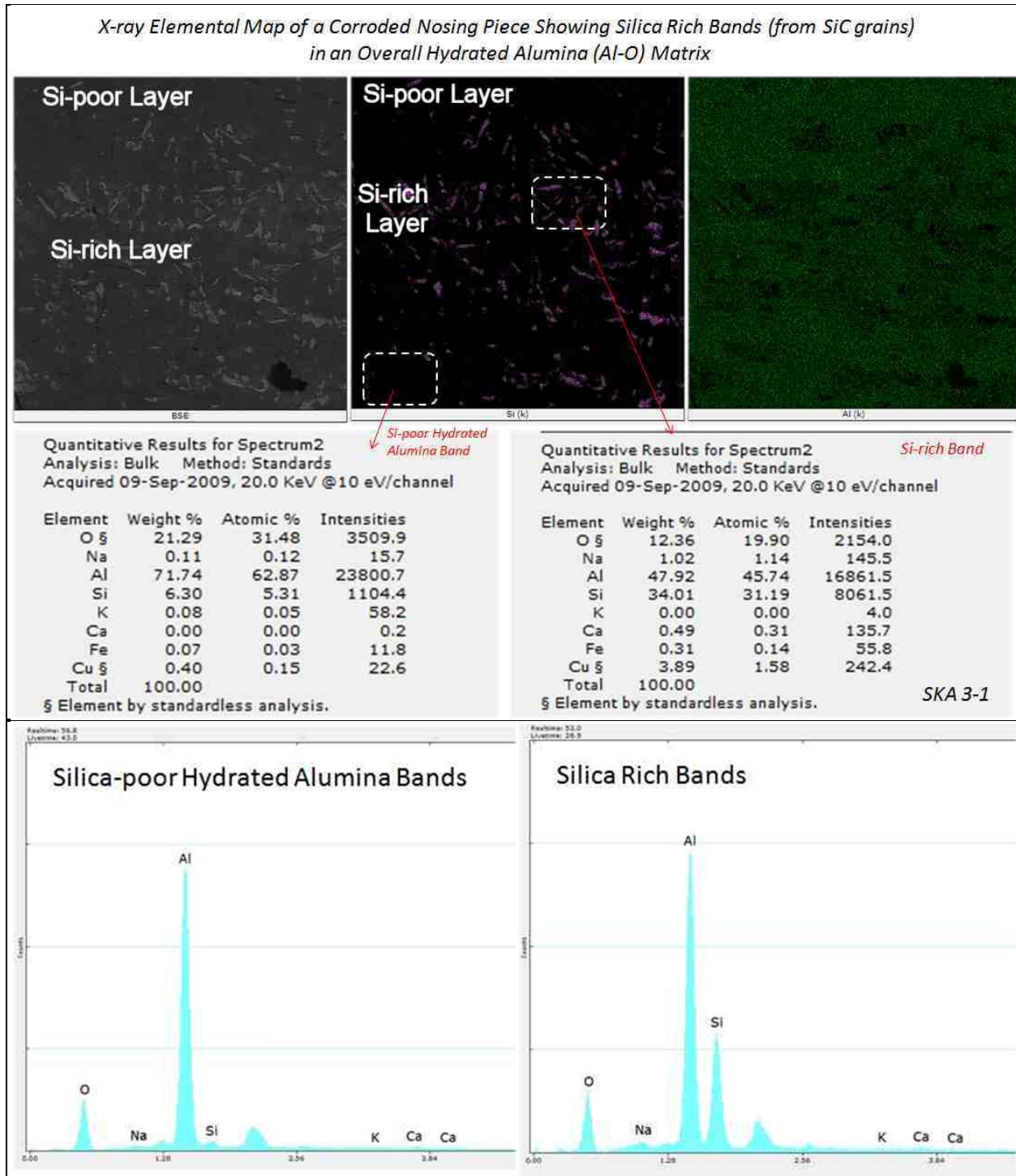


Figure 10: X-ray elemental maps and elemental analyses of areas from silicon-rich and silicon-poor aluminum rich bands.

Preferential Corrosion & Cracking of Aluminum Nosing at the Steel Anchors in SKA 3-2

Figure 11 shows a debonded nosing piece from Sample SKA 3-2 (the top photo shows the underside of the nosing and the bottom photo shows corresponding exposed walking surface of the nosing). Two features are apparent from this figure – (a) preferential location of corrosion of nosing underside at the steel anchors locations, where white corrosion products were formed around the hole in nosing in the right side of photos, where steel components have anchored the nosing to the stair; and (b) radial cracking of the nosing plate itself from reduction in cross sectional thickness of nosing by galvanic corrosion of nosing at the steel interface, in the presence of chloride from the application of deicing salts on concrete stairs.

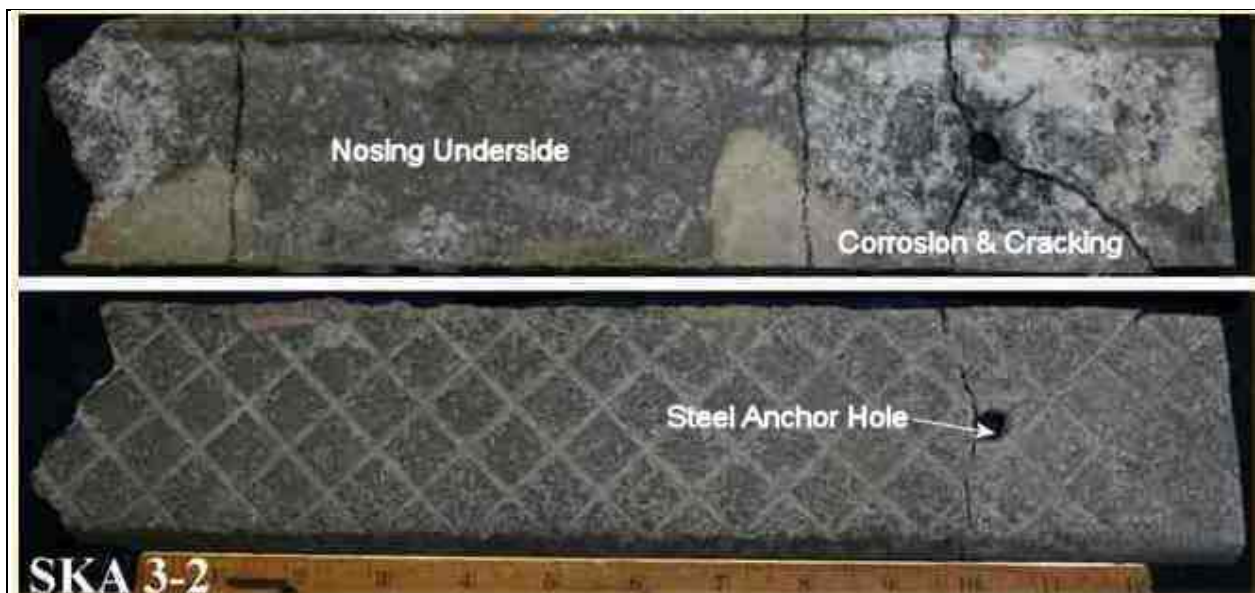


Figure 11: Preferential corrosion of nosing underside at the location of a steel anchor bolt, and cracking by reduction in thickness from corrosion.

Banded & Gelatinous Nature of the Nosing Corrosion Products in SKA 3-2

Figures 12 through 14 show the characteristic banded microstructure of individual sheet-like pieces of corrosion products from nosing in Sample SKA 3-2, which was also evident in Sample SKA 3-1. Plastic bags of loose samples received with the above corroded nosing plate contained many small pieces of nosing corrosion products, which are soft, friable, sheet-like layered masses of corroded metal.

Cross sections of those corroded metal pieces show unique banded microstructure (Figure 12) of alternating layers of white deposits and dark corroded metal. The light (white) and dark (gray) alternating bands are very distinct and similar to gneissose structure seen in gneiss. The

dark bands are rich in silicon phases, whereas the light white bands are rich in hydrated alumina corrosion products.

Blue dye-mixed epoxy-impregnated thin section of those corroded metal pieces reveal the banded microstructure in great detail – showing the alternating dark and light bands, as found in the corrosion products from Sample SKA 3-1 (Figure 9). Figures 13 and 14 show this banded microstructure in thin section as seen through a petrographic microscope at high magnification and a stereomicroscope at relatively low magnification, respectively – in both cases light was transmitted through the thin section. The tables following the figures show compositional variations of white deposits that were collected from the sample as powders or small flakes.

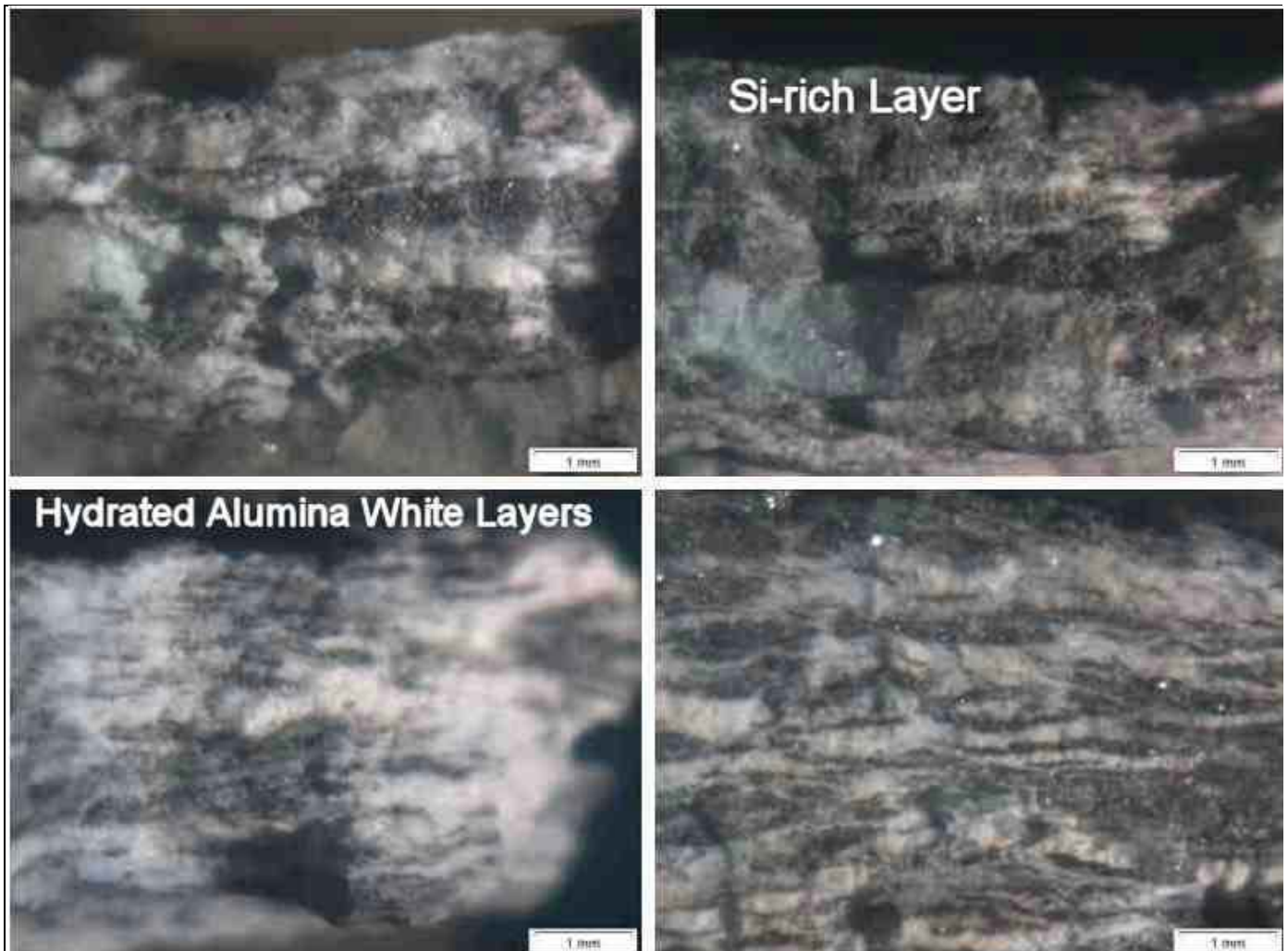


Figure 12: Banded nature of individual pieces of nosing corrosion products showing alternating bands of white deposits and dark hydrated aluminum layers on the fresh fractured cross sections.

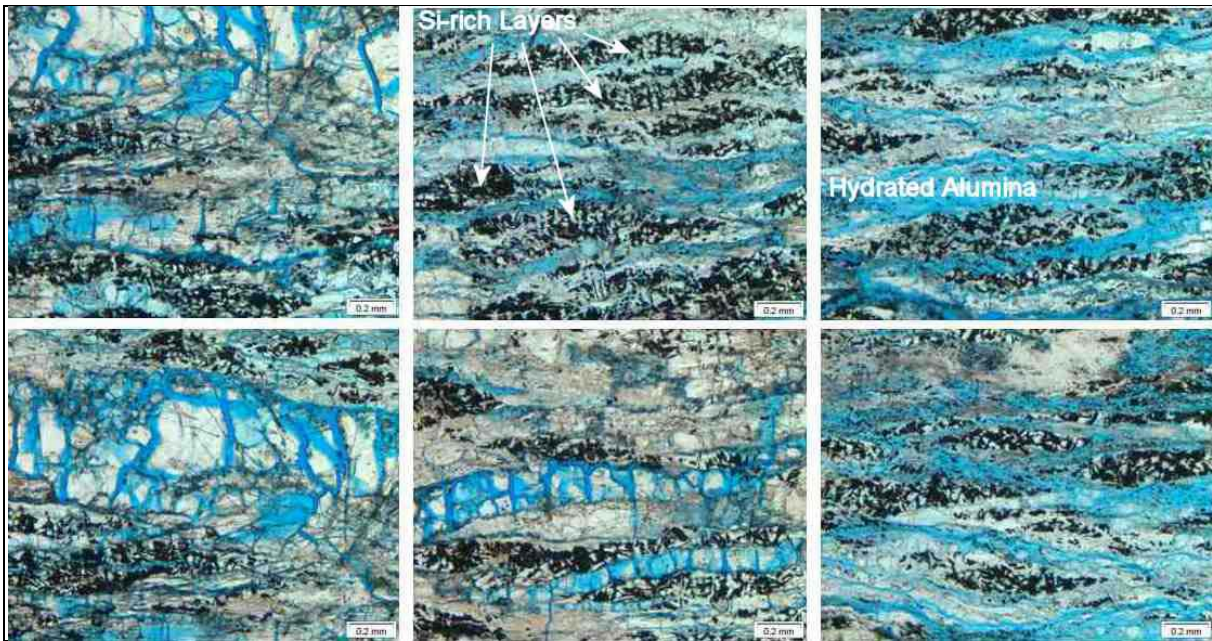


Figure 13: Transmitted light photomicrographs of banded microstructure of nosing corrosion products showing alternating bands of silicon and aluminum-rich phases.

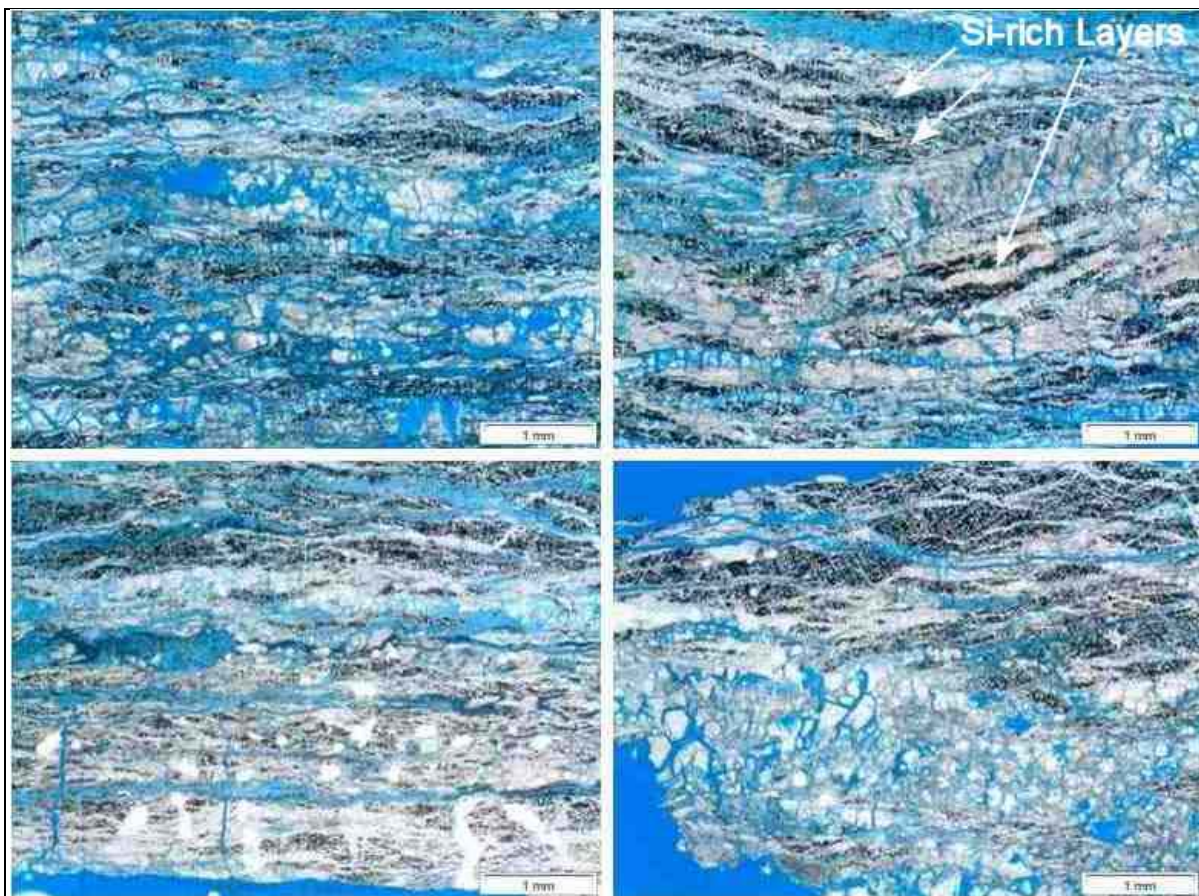


Figure 14: Transmitted light photomicrographs of banded microstructure of nosing corrosion products showing alternating bands of silicon and aluminum-rich phases.

In a petrographic microscope (in cross polarized-light mode), the white deposits show a completely optically isotropic nature, which is indicative of its gelatinous (amorphous) nature. The deposits resemble typical alkali-silica reaction gel in a concrete in terms of isotropic masses of deposits with numerous shrinkage microcracks transecting the masses. The following backscatter electron image of epoxy-impregnated polished cross section of a corroded nosing piece (received as a small friable piece) confirms its sheet-like layered structure with numerous parallel microcracks, and alternating bands of silicon-rich (marked with arrows) and silicon-poor hydrated aluminum layers.

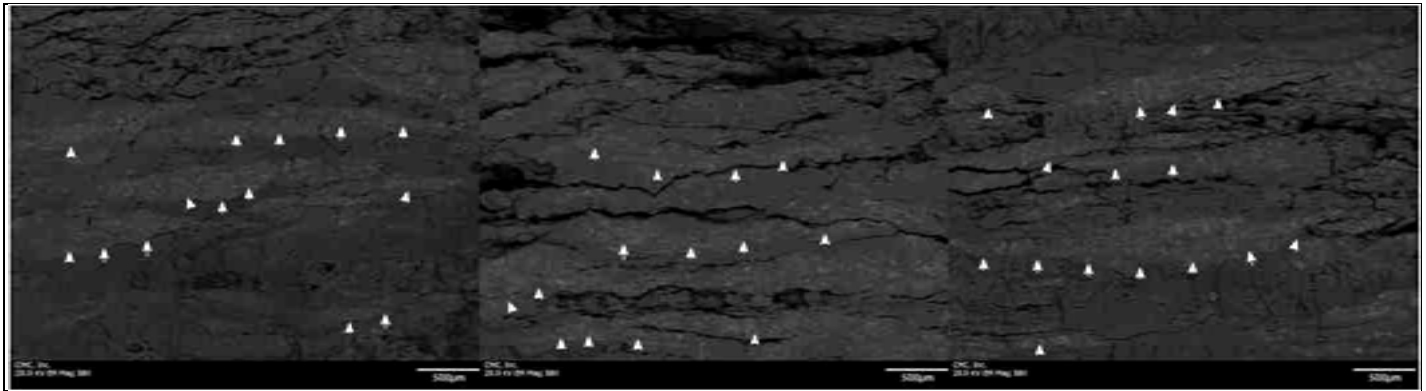


Figure 15: Backscatter electron images of aluminum nosing corrosion products in SKA 3-2 showing its flake or sheet-like nature with parallel microcracks and alternating bands of silicon-rich (arrows) and silicon-poor layers.

An enlarged view of one of the photos in Figure 15 is shown in Figure 16 where numerous parallel and perpendicular microcracks and alternating bands of silicon-rich layers (arrows) and silicon-poor layers are distinct. White layers in Figure 12 correspond to the hydrated aluminum/silicon-poor layers in the backscatter and elemental maps in Figures 16 and 17, and alternating dark bands in Figure 12 layers correspond to the silicon-rich layers in Figures 16 and 17. Figures 15 and 16 are not of the corroded bottom layer of the nosing but from a separate small sheet-like friable piece of the corrosion products that was received in a plastic bag.

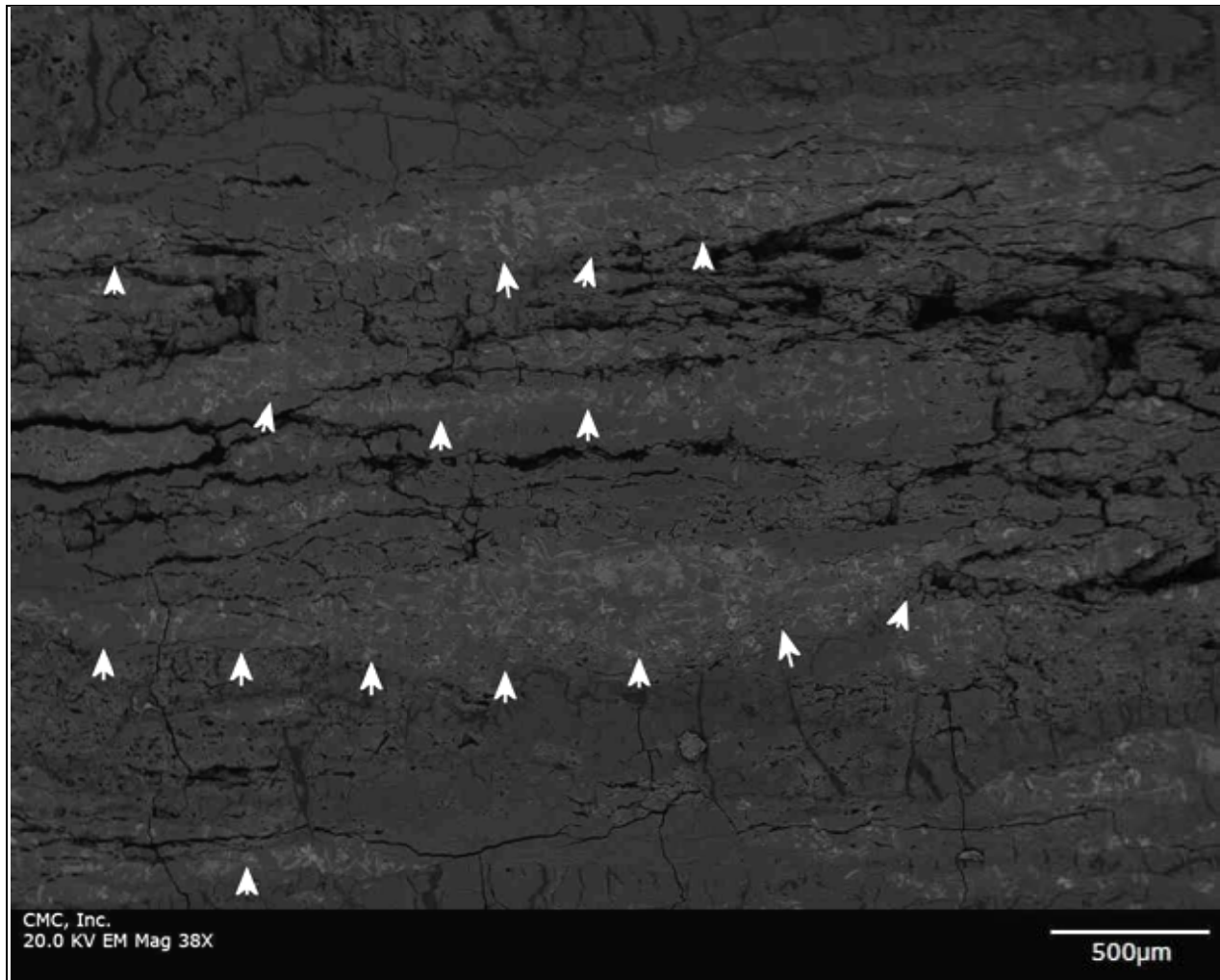


Figure 16: An enlarged view of the right BSE image in Figure 15 showing parallel microcracks and alternating bands of silicon-rich (arrows) and silicon-poor layers in a sheet-like corrosion product of aluminum nosing.

SEM-EDS elemental analyses of silicon-rich layers, a silicon-rich phase, and silicon poor hydrated aluminum layers show the following general compositions (in atomic weight percent):

Areas	Al	Si	O
Si-Rich Layers	18.1	17.9	63.5
Si-Rich Phase	0.5	32.9	66.6
Si-Poor Layers	22.1	1.9	63.6

Figure 17 shows detailed compositional analyses and x-ray elemental mapping of silicon-rich layers and silicon-poor hydrated aluminum layers in the corrosion product of nosing in SKA 3-2, where the left photo shows the BSE image, and middle and right photos show corresponding elemental mapping of distribution of silicon and aluminum, respectively:

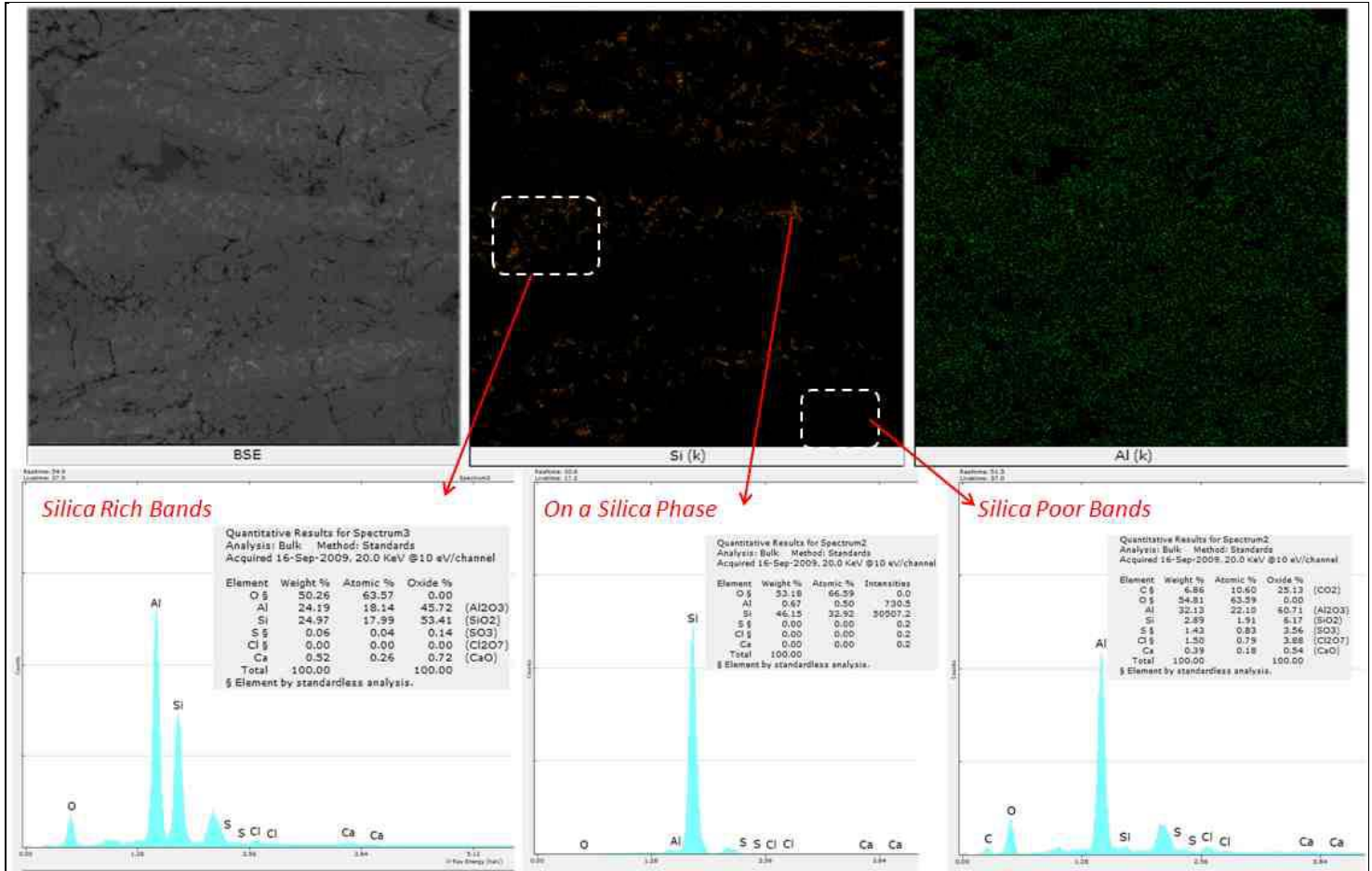


Figure 17: BSE image and corresponding silicon and aluminum distribution maps showing the banded nature of silicon-rich and silicon-poor layers.

The silicon-rich layers are due to the use of silicon carbide grains embedded in the molten metal matrix during the manufacturing of nosing, which are denser, darker, and significantly harder than the alternating silicon-poor hydrated aluminum layers (which are soft, powdery and white). Such banded arrangement of silicon-rich and silicon-poor layers in the corroded products is due to severe corrosion of metal in the alkali hydroxide solution from concrete. In the sound metal body no such banding is observed, where silicon-rich areas are uniformly distributed over a metal matrix. This banded arrangement of layers is distinct in corrosion products in both Samples SKA 3-1 (Figures 9, 10) and SKA 3-2 (Figures 12-17).

The following table lists variations in chemical compositions of white deposits collected as small powders or fine flakes from various pieces of corroded nosing in Sample SKA 3-2 that were analyzed by SEM-EDS. In all cases, overall abundance of aluminum and oxygen, indicating the basic hydrated aluminum composition of the corrosion product is evident, in which various incorporations of silicon, calcium, magnesium, chlorine, etc. are detected.

Elements	1	2	3	4	5	6	7
Al	19.5	25.4	32.6	33.3	28.5	30.7	11.5
O	60.3	65.2	61.1	62.2	60.9	61.0	60.4
Si	1.1	1.0	1.7	2.0	6.9	0.4	8.9
Ca	6.2	0.0	0.7	0.1	3.2	0.0	9.0
Mg	3.2	0.0	0.0	0.0	0.0	2.5	4.1
Cl	0.0	5.1	0.1	2.0	0.3	0.6	0.0
S	0.0	0.8	0.1	0.3	0.0	0.1	0.0
Comments on Possible Phases	Hydrated Alumina Corrosion Product with some Ca-Mg-Si	Hydrated Alumina Corrosion Product with some Cl & Si	Hydrated Alumina Corrosion Product with some Si	Hydrated Alumina Corrosion Product with some Cl & Si	Hydrated Alumina Corrosion Product with some Si, Ca	Hydrated Alumina Corrosion Product with some Mg-Si-Cl	Hydrated Alumina Corrosion Product with some Ca-Mg-Si

XRD Evidence of Aluminum Hydroxide Phases in Gelatinous Mass of Nosing Corrosion Products

Despite the overall optically amorphous nature of white corrosion products of aluminum nosing, x-ray diffraction studies of the corrosion products detected a few low-intensity peaks of crystalline phases of aluminum hydroxide [Bayerite and Gibbsite $\text{Al}(\text{OH})_3$, and Boehmite $\text{AlO}(\text{OH})$], along with minor to trace amounts of calcite [CaCO_3] and Nantokite [CuCl] (Figure 18). Detection of bayerite in concrete from aluminum corrosion is not uncommon [4], where bayerite forms as metastable phase between amorphous hydrated aluminum and monoclinic gibbsite. Occurrences of aluminum hydroxide phases, i.e. bayerite, gibbsite, and boehmite were previously described in other studies [4], where aluminum hydroxide initially form as bayerite, which is metastable and is reportedly an intermediate stage between amorphous hydrated aluminum and monoclinic gibbsite. Both bayerite and gibbsite form of aluminum hydroxide are found (where gibbsite is previously reported in Ref. 4 to form at advanced stage at the expense of bayerite), as well as a metastable phase boehmite, which, reportedly, forms at an initial stage from soluble hydroxyl aluminate ions [$\text{Al}(\text{OH})_4^-$] prior to the formation of bayerite and gibbsite [4]. Detection of a minor Nantokite (CuCl) phase in the pattern is not surprising from the detection of Al-Cu alloy phases in the corroded base of nosing (Figure 7) and the presence of chloride in the concrete.

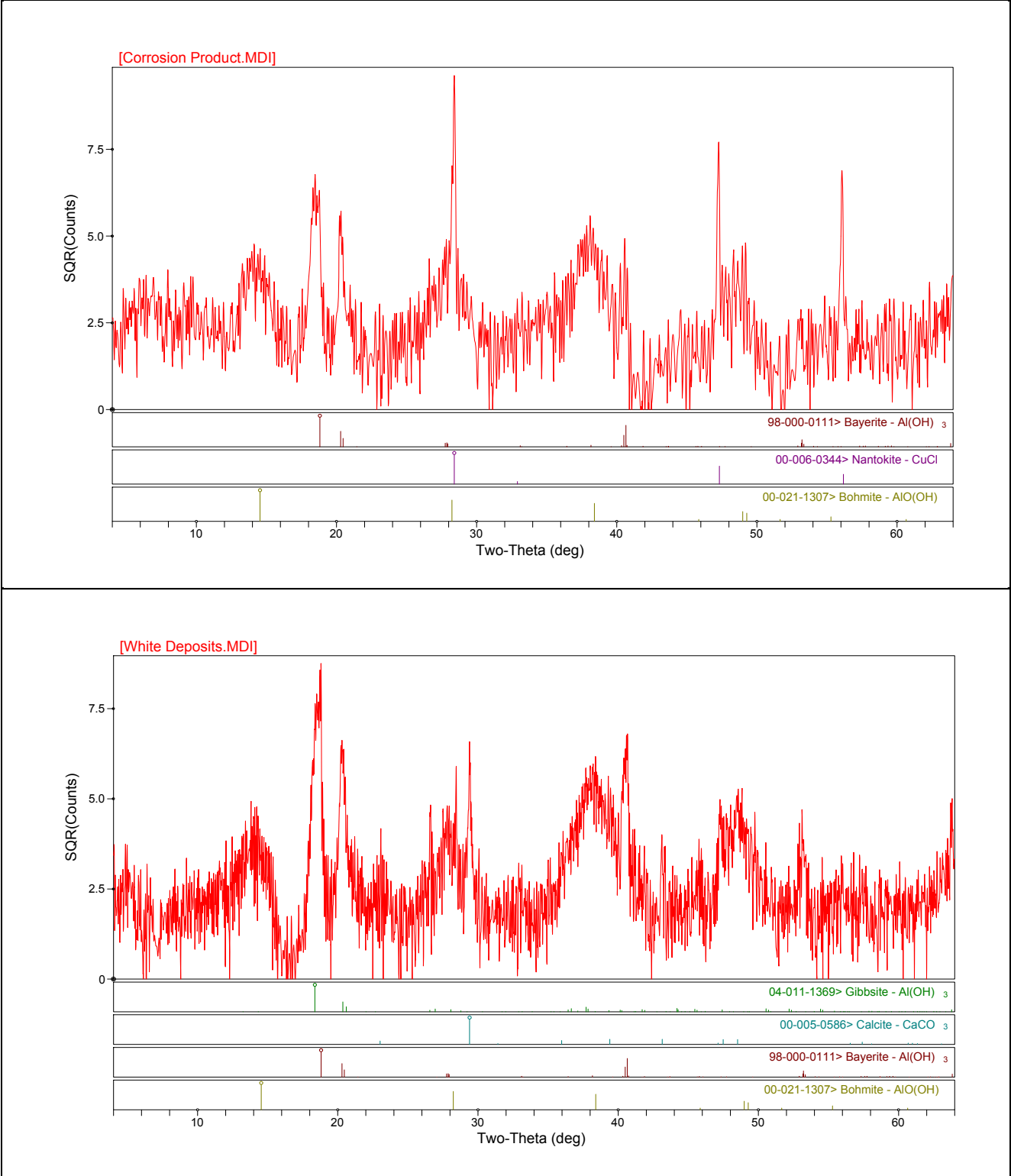


Figure 18: X-ray diffraction patterns of white corrosion products collected from two samples showing the presence of aluminum hydroxide (bayerite, gibbsite, and boehmite) crystals in an overall gelatinous mass.

Concrete Stairs and Repair Patches

The concrete poured in stairs is air-entrained (Figure 19, top row) and made using crushed granite coarse aggregate having a nominal maximum size of $\frac{3}{4}$ in., natural siliceous sand fine aggregate having a nominal maximum size of $\frac{3}{8}$ in., a cementitious materials content estimated to be equivalent to $5\frac{1}{2}$ to 6 bags of portland cement per cubic yard of which 10 to 15 percent is estimated to be fly ash, a water-cementitious materials ratio estimated to be 0.40 to 0.45, and an air content estimated to be 4 to 5 percent. This was consistent with recovered mixture designs. Both coarse and fine aggregate are well-graded, well-distributed, and have been sound during their service in the concrete. The concrete reportedly had about 2 to 3 gallons of calcium nitrite based corrosion inhibitor included during mixing. There is no evidence of any physical or chemical deterioration of concrete *per se* or its ingredients (e.g., freezing-related distress, alkali-aggregate reaction, etc.) detected in the samples that can cause distress to the nosing. The only evidence of chemical deterioration detected in concrete is the chloride-induced corrosion of steel anchor embedded in concrete, where the determined high chloride contents of concrete stairs near the surface have initiated corrosion of steel anchor.

Repair materials (Figure 19, bottom row) used as patches in an attempt to hold debonded nosings to the concrete in previous repair attempts are determined to be dense, hardened neat paste or mortar of portland cement plus limestone fine based cementitious materials, with or without fine quartz sand (1 mm nominal size), which are judged ineffective in preventing nosing corrosion and de-bonding that have occurred from inside, i.e. from underlying steel anchor/nut/bolt in the presence of chlorides and moisture in the concrete.

Neither the repair materials or the portland cement concrete substrate is judged to have any direct influence on the deterioration of the nosings from concrete materials-related distress because similar concrete was used at all stair locations and only a portion of the stair nosings were in an advanced state of distress. These areas reportedly coincided with areas that receive more foot traffic and therefore could be exposed to more transient salts.

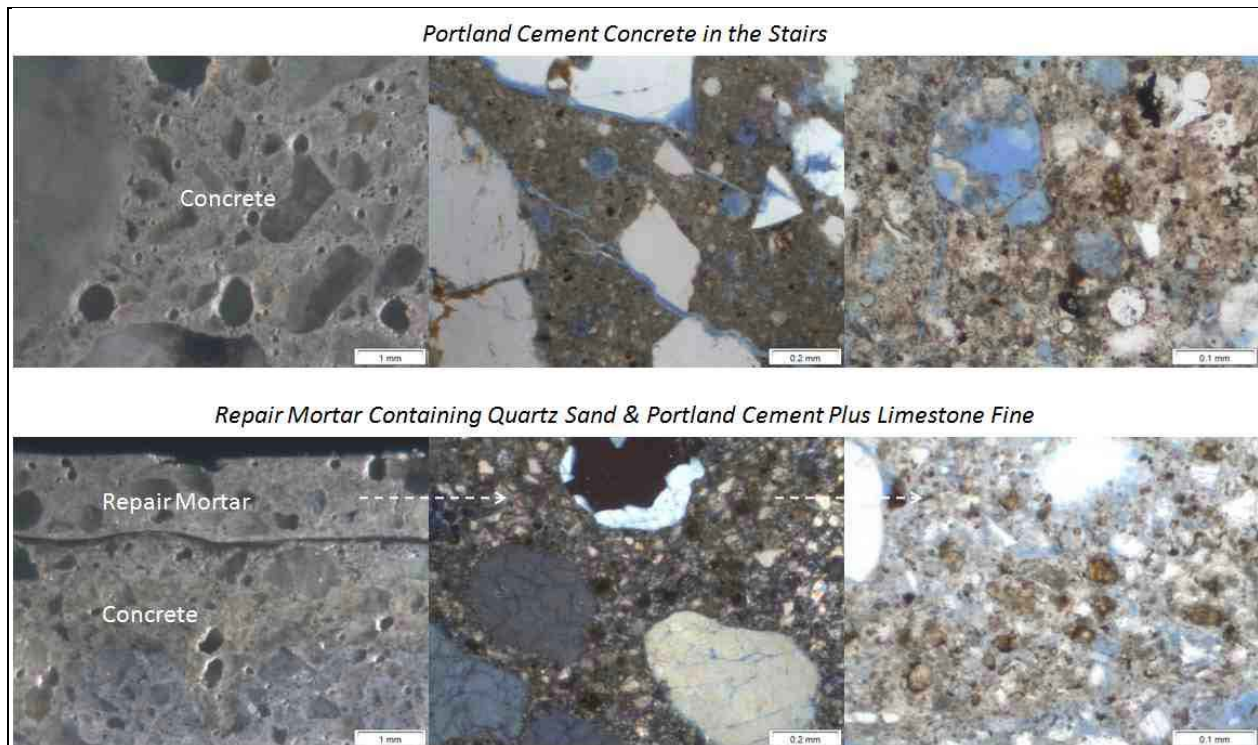


Figure 19: Photomicrographs of lapped cross section (left), and thin section (middle and right) of concrete (top photos) and repair mortar (bottom photos) showing air-entrained concrete containing sand and crushed stone aggregates, and portland cement and fly ash particles in paste, and fine quartz sand, portland cement, and limestone fine particles in a dense repair mortar coat applied on concrete.

Discussion

Corrosion of Aluminum Nosing and Corrosion Products

Silicon carbide grains embedded on the walking surface of aluminum nosing created a uniform distribution of silicon-rich phases in the aluminum matrix over the entire thickness of the nosing up to the depth of the corroded base, adjacent to the concrete.

Corrosion of aluminum nosing along the base, in contact with alkali hydroxide and chloride solutions in concrete created blade-shaped silicon-rich phases in a hydrated aluminum metal matrix with occasional phases of Al-Si-Fe and Al-Cu compositions.

Further corrosion of metal has caused a significant loss of strength, cracking, and created soft, friable, sheet-like layered mass of highly corroded metal, with alternating bands of dense and dark silicon-rich layers from preferential alignment of silicon-rich phases in a layer, and layers of soft, powdery white deposits of gelatinous hydrated aluminum layers with finely crystalline phases of aluminum hydroxide (gibbsite, bayerite). These progressive changes in microstructure

from the sound metal to sheet-like corroded metal corrosion product can be shown by the BSE image and corresponding Al-Si distribution maps in Figure 20, and in the schematic diagram in Figure 21 illustrating possible process of formation of sheet-like corrosion products through metal dissolution in solution (the *through solution* process of aluminum corrosion).

Formation of an overall gelatinous (amorphous) mass of hydrated aluminum corrosion products has created expansion and associated cracking of concrete and debonding of aluminum nosing from the concrete. Corrosion process of aluminum initially forms the gelatinous hydrated aluminum mass, from which microcrystalline masses of boehmite, bayerite, and gibbsite can form with advanced stages of corrosion. Formation of the gelatinous mass itself is responsible for the expansion and cracking in adjacent concrete. A reduction in thickness of nosing from corrosion has caused cracking of the nosing itself. Evolution of hydrogen gas due to alkali hydroxide attack of aluminum from concrete can also create a porous zone at the aluminum-concrete interface, as was reported by Ref. 4.

Preferential occurrences of aluminum corrosion and formation of corrosion products at the locations of steel anchors indicate galvanic corrosion of aluminum in contact with steel, especially in the presence of high chlorides, detected at the top portion of concrete stairs from the reported applications of chloride-containing deicing salts.

A typical ring-structured corrosion product around the steel nuts, bolts, and anchors were detected after removing the nosing plates. The product consists of: (a) reddish brown corrosion products of steel anchor and nut/bolt in concrete in the presence of chloride, oxygen, and moisture, which are surrounded by (b) white corrosion products of hydrated aluminum from nosing at the locations of coupling to steel anchor, where aluminum corrosion was enhanced by the presence of chloride. It is hypothesized that corrosion of the steel components might have started after the aluminum corrosion products created a barrier in the direct vicinity of the connection, or once the steel became atmospherically exposed in the presence of chlorides from associated aluminum distress.

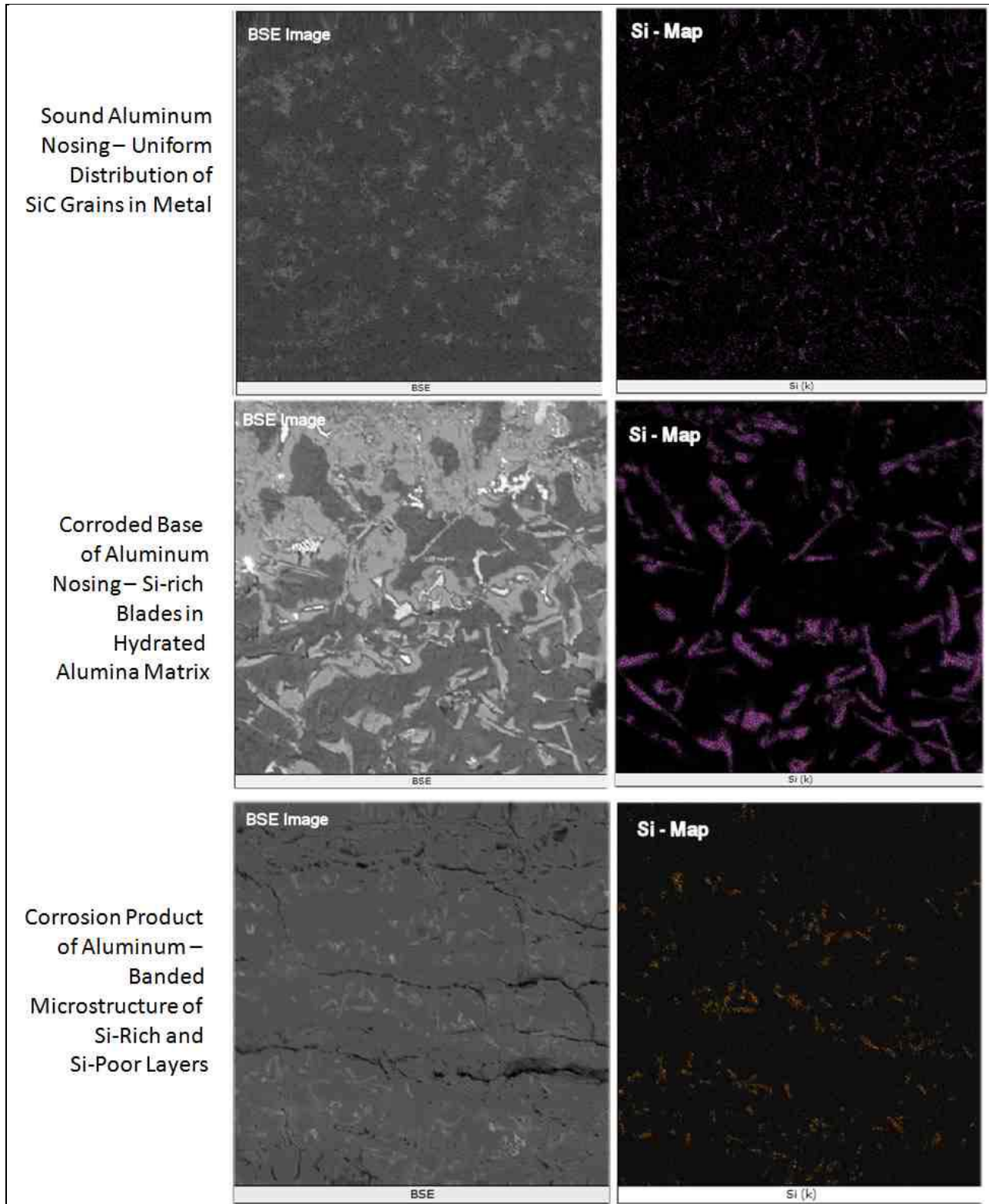


Figure 20: Progressive change in microstructure of aluminum-silicon distribution from uniform distribution of Al and Si in the sound metal nosing (top) to blade-shaped silicon-rich phases at its corroded base (middle) to sheet-like corrosion product showing banded microstructure with layered arrangement of silicon-rich (dashed lines) and silicon-poor phases (bottom).

Mechanism of Formation of Sheet-like Banded-Microstructure of Nosing Corrosion Products

The following schematic diagram in Figure 21 illustrates a possible mechanism of formation of a sheet-like banded microstructure of severely corroded nosing by layer-by-layer dissolution of the original aluminum nosing by alkali hydroxide solution from the concrete, followed by layer-by-layer density settlement of hard silicon-rich phases (from original embedded SiC granules) and soft hydrated aluminum corrosion products on top of silicon-rich phases:

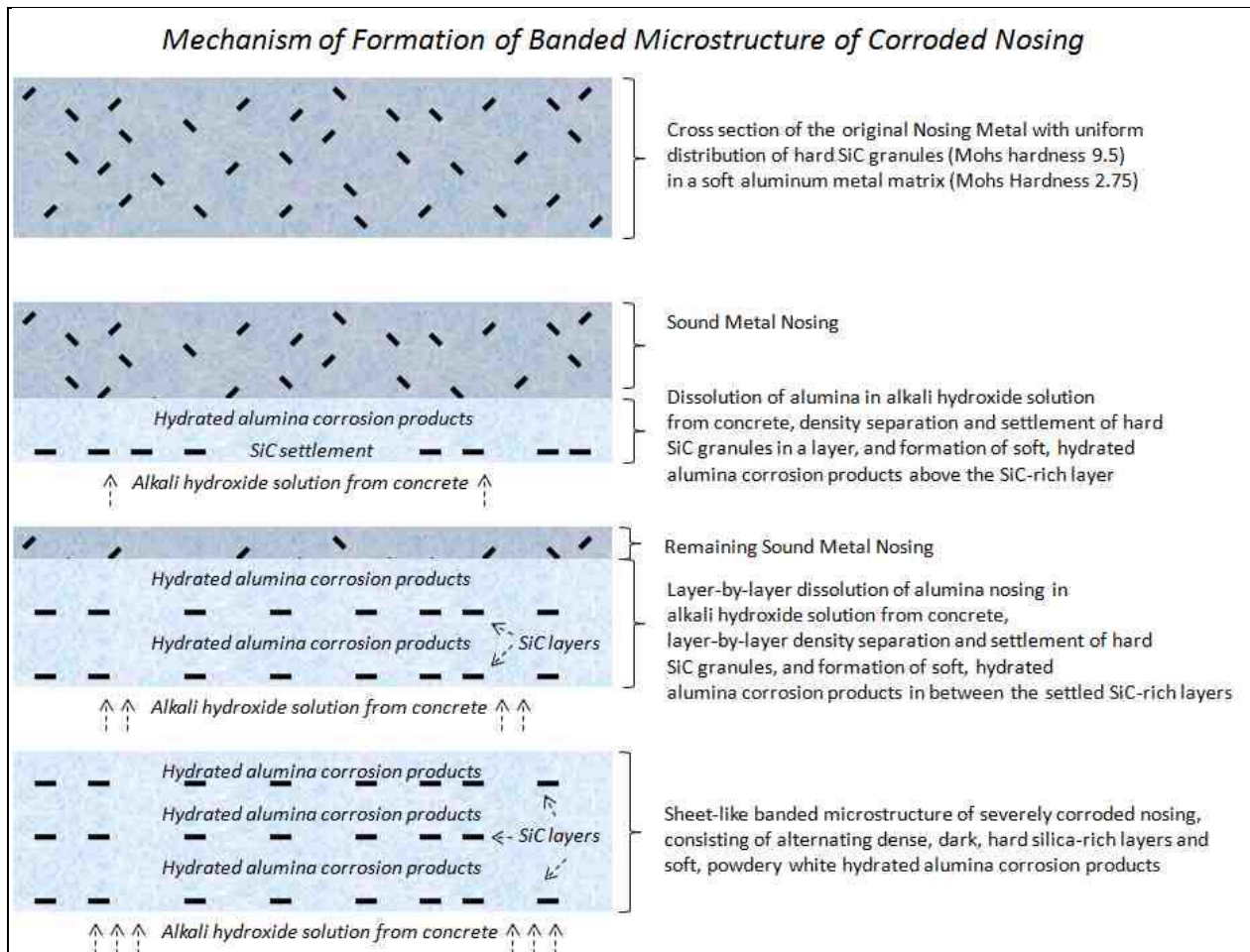


Figure 21: Schematic diagram of formation of banded microstructure and sheet-like corrosion product of nosing.

Such a banded microstructure is the result of embedding a very hard material (silicon carbide granules having Mohs hardness of 9.5) in a very soft aluminum metal matrix (Mohs hardness of 2.75), and is indicative of formation of corrosion products by dissolution of the original metal in alkali hydroxide solution, followed by density settlement of hard silicon-rich phases in the solution to form a silicon-rich layer beneath the relatively less dense layer of hydrated

aluminum corrosion products. This *through-solution* mechanism of the corrosion process is best evidenced by this banded microstructure of two materials having different hardness.

Mechanism of Corrosion of Aluminum in Concrete not in Electrical Connectivity to Steel, and Galvanic Corrosion of Aluminum in Concrete that is Coupled to Steel

The following two schematic diagrams (Figures 22 and 23) illustrate the mechanism of corrosion of aluminum in a portland cement concrete in a case where the metal is not electrically connected (coupled) to steel (Figure 22), and in a case similar to the present one where aluminum is coupled to steel and exposed to moisture and chloride for galvanic corrosion (Figure 23):

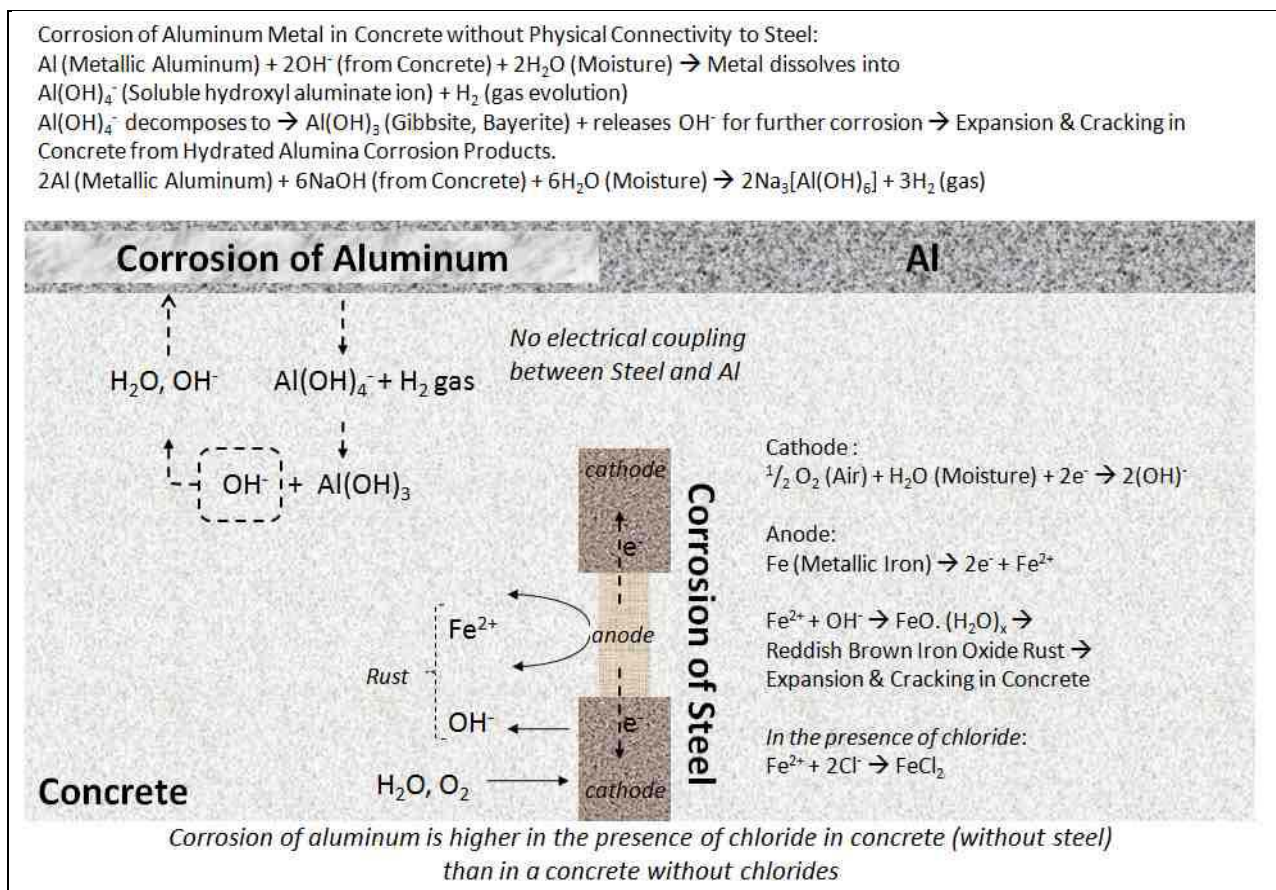


Figure 22: Mechanism of corrosion of aluminum metal in concrete without electrical connectivity to steel.

Steel embedded in concrete does not typically corrode due to the formation of a passive layer over the steel surface in high pH environments. When the passive layer is destroyed, for instances, from a lowering of the pH from carbonation or the presence of sufficient quantities of chlorides, corrosion of steel may occur, with the rate being dependent on several factors.

Corrosion of steel in concrete releases electrons at the anode, which flow to the cathode, and combine with moisture and oxygen to form hydroxyl ions. Hydroxyl ion and/or chloride combines with oxidized iron at the anode to form iron hydroxide and chloride corrosion products, further oxidation of hydroxide forms various iron oxide corrosion products with a volume expansion of 2 to 6 times the original volume of iron metal (depending on the corrosion product that forms), and associated cracking of concrete. Corrosion can occur in the presence of chloride even at a high pH where chloride ions penetrate through the protective oxide film around iron and causes pitting-type corrosion.

Unlike steel, which is generally protected at the high pH environment of portland cement concrete by an iron oxide film, corrosion of aluminum is rapid in the high pH environment of moist concrete, where hydroxyl ions from concrete's pore solution dissolve aluminum metal (including its protective oxide passive layer) and form soluble hydroxyl aluminum ions and evolve hydrogen gas. The hydroxyl aluminum ion forms a gelatinous hydrated aluminum mass, from which various aluminum hydroxide crystals (initially boehmite, followed by bayerite, and then gibbsite) can form with advanced stages of corrosion. This type of corrosion is common in an amphoteric metal, such as aluminum, which shows corrosion at the cathodic portion of metal surface because of the build up of alkalis caused by the cathodic electrochemical reactions.

In galvanic corrosion of aluminum coupled to steel, hydroxyl ion for dissolution of aluminum comes not only from concrete but also from corrosion of steel in concrete (from cathode), which aggravates aluminum corrosion process compared to the case with no steel or no coupling with steel. The galvanic reactions between aluminum and iron cause preferential loss of more anodic aluminum and preservation of the more cathodic steel, where chloride ions act as catalyst to sustain the process and aluminum corrosion. This is similar to the use of sacrificial zinc or aluminum anodes connected to reinforcing steel to preserve reinforcing steel and extend the service life. Aluminum releases electrons at the anode (electrons conduct through metals to iron at cathode), receives hydroxyl ions from iron cathode by ionic conductivity through concrete, and forms aluminum hydroxide. This reaction is similar to typical galvanic corrosion of aluminum coupled to copper in buried power or telephone cables. The presence of moisture and chloride are both essential to sustain the galvanic process (both galvanic and stray current corrosion), which are indeed present in a moist outdoor environment of concrete exposed to chloride-containing deicing salts.

Galvanic Corrosion of Aluminum Metal Coupled (Physically Connected) to Steel in Concrete - Aluminum Corrodes more (sacrificial metal) at the expense of steel by Galvanic Corrosion by:

Aluminum Anode: $\text{Al} \rightarrow 3\text{e}^- + \text{Al}^{3+}$;

Steel Cathode: $\frac{1}{2} \text{O}_2$ (Air) + H_2O (Moisture in Concrete) + 2e^- (from Aluminum Anode) $\rightarrow 2(\text{OH})^-$

Alumina Hydroxide Formation: $\text{Al}^{3+} + 3\text{OH}^-$ (from both concrete and steel) $\rightarrow \text{Al}(\text{OH})_3$

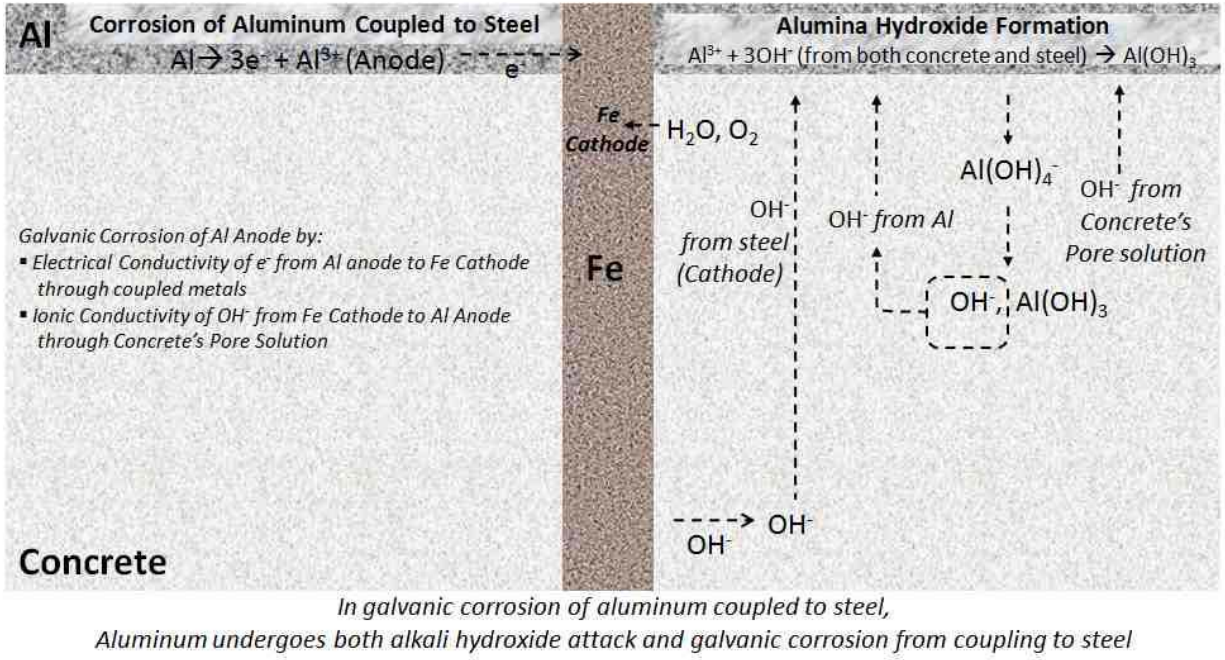


Figure 23: Mechanism of galvanic corrosion of aluminum metal in concrete coupled to steel.

Conclusion

Field evidence, coupled with detailed petrographic examinations of aluminum nosing corrosion, products of corrosion, and related distress in nosing and concrete illustrate the importance of proper protection of aluminum metal with an inert or insulating (e.g., bituminous) coating when used in a highly alkaline environment of portland cement concrete, especially in an outdoor environment in the presence of chloride (e.g., from chloride-containing deicers) and steel electrically connected to aluminum. Nosing surfaces directly attach to concrete stairs generally did not show any corrosion or corrosion-related distress. It is only at the locations of steel anchors to the nosing, where aluminum nosing show severe corrosion, thickness reduction, metal fracturing, and formation of corrosion-related hydrated aluminum products with concomitant debonding (bowing) of metal from concrete, mainly at locations in between two steel anchors. Formation of a gelatinous (amorphous) corrosion product of nosing, along with some crystalline aluminum hydroxide phases are judged to have the potential to cause expansion by moisture absorption and associated lifting of the nosing from the nosing-concrete interface.

Acknowledgments

Sincere thanks are due to Dr. Chris Bagnall, editor-in-chief of *Materials Characterization* and a Fellow of ASM International for detailed review and various comments on the article, Mitzi Casper (CMC) for sample preparation and photomicrography, and Jennifer L. Hall (CMC) for review and formatting of the final manuscript.

References

1. Wright, T.E., "An unusual case of corrosion of aluminum conduit in concrete," *The Engineering Journal*, V 38, No. 10, 1357-1362, 1955.
2. Monfore, G.E., and Ost, Borje, "Corrosion of aluminum conduit in concrete," *Journal Portland Cement Assoc. Research and Development Laboratories*, Vol 7, No. 1, January, pp. 10-22, 1965.
3. Woods, Hubert, "Corrosion of Embedded Material Other than Reinforcing Steel, Significance of Tests and Properties of Concrete and Concrete-Making Materials," STP No. 169A, 230-238, American Society for Testing and Materials, 1966.
4. Setiadi, A., Milestone, N.B., Hill, J., and Hayes, M., "Corrosion of aluminum and magnesium in BFS composite cements," *Institute of Materials, Minerals and Mining*, 2006.
5. Nurnberger, Ulf, "Corrosion of metals in contact with mineral building materials," *Otto-Graf-Journal*, Vol 12, pp 69-80, 2001.
6. McGeary, F., "Performance of Aluminum in Concrete Containing Chlorides," *Journal of the American Concrete Institute*, V 63, No. 9, 247-265, 1966.
7. "The aluminum and concrete controversy," *Concrete Construction Magazine*, The Aberdeen Group, 1965.
8. ACI Committee 222, "Design and Construction Practices to Mitigate Corrosion of Reinforcement in Concrete Structures (ACI 222.3R-03)," *Manual of Concrete Practice*, The American Concrete Institute, Farmington Hills, MI, 29 pp, 2003.
9. ACI Committee 318, "Building Code Requirements for Structural Concrete (ACI 318-08)," *Manual of Concrete Practice*, The American Concrete Institute, Farmington Hills, MI, 465 pp, 2008.